Chapter 5
Engineering Upconversion Nanoparticles for Multimodal Biomedical Imaging-Guided Therapeutic Applications

Wenpei Fan, Jianlin Shi, and Wenbo Bu

Abstract As one of the most important branches of nanotechnology, nanotheranostic medicine that aims at integrating diagnostic/therapeutic functions in one system is expected to provide novel strategies for accurate imaging-guided therapy of human major diseases like cancer. Among various inorganic or organic theranostic probes, lanthanide-doped upconversion nanoparticles (UCNPs) demonstrate superior advantages in upconversion luminescent imaging by contrast with traditional luminescent probes as well as great potential in the development as multimodal imaging (e.g., magnetic resonance imaging, computed tomography imaging, etc.) probes by the selective doping of various functional ions (e.g., Gd^{3+}, Yb^{3+}, Ho^{3+}, etc.). Furthermore, by suitable surface engineering (e.g., mesoporous silica coating, biological molecule conjugation etc.), UCNPs can simultaneously serve as delivery vehicles of drugs/photosensitizers for multimodal therapeutic applications (e.g., chemotherapy, photodynamic therapy, etc.) under the above significant multimodal imaging guidance. Herein, we summarize and discuss the very recent progresses in the engineering of UCNPs for multimodal imaging-guided therapeutic applications.

Keywords Upconversion nanoparticles • Nanotheranostic medicine • Hydrophilic modification • Multimodal imaging • Synergetic therapy • Imaging-guided therapy

5.1 Introduction

As a new generation of luminescent probes, lanthanide-doped upconversion nanoparticles can convert low-energy/long-wavelength near-infrared (NIR) light into high-energy/short-wavelength visible or ultraviolet (UV) light [1, 2]. Unlike

W. Fan • J. Shi • W. Bu (✉)
State Key Laboratory of High Performance Ceramics and Superfine Microstructures, Shanghai Institute of Ceramics, Chinese Academy of Sciences, 1295 Ding-xi Road, Shanghai 200050, People's Republic of China
e-mail: wbbu@mail.sic.ac.cn

Z. Dai (ed.), *Advances in Nanotheranostics I*, Springer Series in Biomaterials Science and Engineering 6, DOI 10.1007/978-3-662-48544-6_5

the traditional organic dyes or quantum dots that need ultrashort-pulsed laser excitation due to their nonlinear multiphoton absorption, UCNPs can be excited by low-cost continuous-wave diode laser for upconversion luminescence emission [3]. More importantly, UCNPs demonstrate unique advantages in upconversion luminescent (UCL) imaging that could not be achieved by other luminescent probes, such as high sensitivity, superior photostability, large anti-Stokes shift, sharp emission bandwidths, extremely weak autofluorescence, deep penetration of NIR light excitation, and so on [4–7]. Besides, by doping various rare earth ions (e.g., Er^{3+}, Tm^{3+}, Eu^{3+}, Tb^{3+}, etc.) into the UCNPs lattice, diverse wavelengths of UV/vis light can be simultaneously emitted for multicolor luminescent imaging upon a single NIR source excitation [8–10].

Another unique feature of UCNPs in bio-imaging is the realization of multimodal imaging by incorporating special functional ions into the crystal lattice. For example, Gd^{3+}-doped UCNPs can be used as contrast agents for magnetic resonance imaging (MRI) [11, 12]. The doping of some high-Z heavy metal ions (e.g., Yb^{3+}, Ba^{3+}, Bi^{3+}, Lu^{3+}, etc.) can realize enhanced computed tomography (CT) imaging [13–15]. The introduction of some radionuclides like $^{18}F/^{153}Sm$ can offer UCNPs with positron emission tomography (PET) and even single-photon positron emission tomography (SPECT) imaging capabilities [16–19]. Therefore, by the selective co-doping of the above functional ions, multimodal imaging probes based on UCNPs can be successfully designed by integrating MRI/UCL/CT/PET modalities in a single system, which may contribute to future accurate diagnosis of big diseases.

By suitable surface engineering, UCNPs can even used for multimodal imaging-guided therapeutic applications. For example, mesoporous silica-coated UCNPs serve as drug vehicles for enhanced chemotherapy [20–23]. Moreover, based on the fluorescence resonance energy transfer (FRET) from UCNPs to some photosensitizers, photodynamic therapy (PDT) [24–28] can be achieved on deep-seated tumors upon NIR irradiation. By the co-delivery of drugs/photosensitizers/radiosensitizers, the three major treatments of chemo-/radio-/photodynamic therapy can be integrated in a single UCNP-based system. Therefore, UCNPs can be developed into the next generation of theranostic medicine for multimodal imaging-guided therapy, which may substantially enhance the diagnostic/therapeutic efficacy.

Herein, we will summarize the latest studies regarding the engineering of UCNPs for multimodal imaging-guided therapeutic applications. The useful strategies for hydrophilic surface modifications of UCNPs are introduced. Particularly, the recent progress of UCNPs in multimodal biomedical imaging (e.g., MR/UCL, MR/UCL/CT, etc.) as well as imaging-guided therapeutic applications (photodynamic therapy, radiotherapy, etc.) are emphasized and highlighted. Finally, the current challenges and future research directions of UCNPs are also outlooked. We hope that this chapter can offer researchers in this field a timely and comprehensive figure of the recent developments in UCNP-based nanotheranostics and attract increasing attentions among researchers in other related fields and even nonspecialists as well.

5.2 Hydrophilic Surface Modification of UCNPs

So far, among the various synthetic approaches for UCNPs, the hydrothermal method and thermal decomposition method are the two widely used strategies for the fabrication of high-quality, single-crystal, monodispersed UCNPs. However, the synthesized UCNPs are usually not soluble in water due to their hydrophobic surface capped by oleic acid (OA) or oleylamine (OM), so the suitable surface modification may be a key step to make UCNPs water dispersible and suitable for the following biomedical functionalization and applications. A variety of surface modification strategies [2, 6, 8] have been successfully adopted to transfer hydrophobic UCNPs into water, and the most frequently used three modification methods (polymer coating, ligand-free synthesis, silica coating) will be briefly discussed in the following sections.

5.2.1 Polymer Coating Modification

Some biocompatible polymers can be capped onto the surface of UCNPs by replacing the OA/OM ligands, which can not only make UCNPs well dispersible in water but also functionalize UCNPs for biomedical use. For example, Yin et al. [29] described a general ligand-exchange method to replace hydrophobic OA ligands at an elevated temperature (~240 °C) in a glycol solvent. Those short-chain hydrophilic polyelectrolyte molecules (such as poly(acrylic acid) (PAA), poly(allylamine) (PAAm), and poly(sodium styrene sulfonate) (PSS)) could be coated on UCNPs based on the strong coordination of their functional groups to the UCNP surface. Van Veggel et al. [30] reported an efficient technique to use the PEG–phosphate ligand for the replacement of OA ligands, thus producing water-dispersible UCNPs that can be further conjugated with various functional biomolecules. Then, they further developed a facile ligand-exchange strategy to use polyvinylpyrrolidone (PVP) to replace OA ligands and transfer UCNPs into water without aggregation by refluxing in 1:1 DMF–DCM at 100 °C for 6 h [31]. More interestingly, Li et al. [32] reported a simple yet versatile method for using the Lemieux–von Rudloff reagent to directly oxidize the oleic acid ligands on the UCNP surface, thus yielding water-soluble and carboxylic acid-functionalized UCNPs capable of conjugating with other proteins. Lin et al. [33] also modified hydrophilic sodium dodecyl sulfate (SDS) on the surface of OA-UCNPs by heating at 60 °C to evaporate the chloroform solution. In addition, other biocompatible polymers, such as PAH [34], PEI [35], HAD [36], 3MA [37], MSA [38], and PAMAM [39], have also been successfully used to replace the OA ligands to render modified UCNP excellent water dispersity/stability, which may also improve the biocompatibility of UCNPs for the following biomedical applications.

5.2.2 Ligand-Free Synthesis Modification

In order to render the original hydrophobic UCNPs water soluble by completely removing the OA ligand, the ligand-free synthesis method has been developed to make the modified hydrophilic UCNPs capable of directly conjugating with those biocompatible molecules with electronegative groups (-COOH, NH_2, etc.) for further biomedical applications. The OA ligand on the surface of UCNPs can be thoroughly removed by acidic treatment or longtime sonication in excess ethanol. For example, Xu et al. [40] found that the OA ligand on the surface of UCNP nanocrystals could be washed away by excess ethanol under ultrasonic for four times. In addition, after being treated with a HCl solution (pH = 4), Capobianco et al. [41] reported that the OA ligand could be removed, thus yielding positively charged ligand-free UCNPs with high stability and dispersity. These synthesized ligand-free UCNPs could be used for further conjugation with biological molecules like heparin [42], TAT [43], etc., which will make UCNPs target the specific tumors or the cell nucleus.

5.2.3 Silica Coating Modification

Due to the high biocompatibility and easy surface modification, inorganic silica was usually coated on the surface of hydrophobic nanocrystals to endow them with high water stability as well as easy conjugation with other functional biomolecules. There are two chemical strategies for the dense silica coating on UCNPs. One is the Stöber method, which can be used to coat uniform silica on the surface hydrophilic UCNPs by the addition of TEOS into mixed solution of water/ethanol/ammonia. For example, van Veggel et al. utilized this method to coat thickness controllable on LaF_3: Yb^{3+}/Er^{3+} nanoparticles [44]. The other is the reverse emulsion method [45–49] that is extensively adopted to coat dense silica on hydrophobic UCNPs. Zhang et al. [50] successfully coated a very thin and uniform dense silica shell on hydrophobic $NaYF_4$:Yb/Er/Tm nanocrystals by using a reverse emulsion method to produce monodisperse $NaYF_4$:Yb/Er/Tm@SiO_2 nanoparticles. Our group [51] also employed this method to coat a thickness-controllable silica shell on $NaYF_4$:Yb/Er nanoparticles by changing the adding amount of TEOS, which was then functionalized with APTES to attach small Au nanoparticles.

In addition to dense silica, mesoporous silica was also frequently coated on UCNPs to fabricate UCNPs@mSiO_2 nanoparticles, which could serve as delivery vehicles of drugs, photosensitizers, etc. As expected, the integration of UCNPs with mesoporous silica can achieve the combination of fluorescent imaging and drug-delivered chemotherapy, which may be developed as a new generation of imaging-guided nanotheranostics. Zhang et al. [25] reported the successful coating of mesoporous silica on UCNPs to encapsulate photosensitizer ZnPc for photodynamic therapy under NIR excitation. Our group [52] coated a thickness-dependent

mesoporous silica shell on UCNPs by simply adjusting the TEOS addition amount. Lin et al. [53] also coated mesoporous silica on CTAB-modified UCNPs to load anticancer drug DOX for targeted imaging and chemotherapy. In a word, the silica coating method may provide an extremely useful platform for fabricating multifunctional UCNP-based nanostructures in addition to the hydrophobic–hydrophilic transition. However, the remaining excess surfactants may cause low colloidal stability and potential toxicity over time. Therefore, the development of more advanced/efficient surface modification strategies that ensure long dispersity/stability of UCNPs in physiological environment will be the next topic of research.

5.3 Engineering UCNPs for Multimodal Biomedical Imaging

After hydrophilic modification, UCNPs can serve as an excellent luminescent probe for in vitro and in vivo UCL imaging due to their incomparable superiorities (e.g., low autofluorescence interference, high photostability, etc.) over quantum dots/organic dyes [54]. Moreover, by the co-incorporating of multiple functional ions (e.g., Gd^{3+}, Ba^{2+}, Mn^{2+}, etc.), UCNPs can be developed into a promising multimodal imaging probe based on the integration of other molecular imaging techniques (MRI/CT/PET/SPECT) with UCL into one single system [8]. Since no single imaging modality is perfect because of its intrinsic drawbacks, the design of multimodal imaging probes by engineering UCNPs may integrate all the advantages of different imaging modalities as well as provide multi-aspect imaging information necessary for the accurate diagnosis in the future.

5.3.1 UCNPs for Single-Modality UCL Imaging

5.3.1.1 UCNPs for Multicolor UCL Imaging

A unique feature lies in UCNPs that their upconversion luminescent (UCL) emission spectra can be well turned by selectively doping various rare earth ions to realize multicolor UCL imaging [55]. For example, by only changing the luminescent ions and adjusting their doping concentrations, Liu's group [56] synthesized a series of PEGylated UCNPs with different UCL emission colors: UCNP1 ($NaY_{0.78}Yb_{0.2}Er_{0.02}F_4$), UCNP2 ($NaY_{0.69}Yb_{0.3}Er_{0.01}F_4$), and UCNP3 ($NaY_{0.78}Yb_{0.2}Tm_{0.02}F_4$). When subcutaneously injected into a rat, multicolor UCL imaging was demonstrated in vivo upon 980 nm laser excitation (Fig. 5.1a). Based on the same method, Hao et al. [57] also realized the tunable multicolor (from blue to white to yellow) fluorescence emission in hexagonal phase $NaGdF_4$: Yb/Tm/Ho nanorobs by simply adjusting the Ho^{3+} concentrations.

Another approach for realizing multicolor UCL imaging is to modulate the luminescence emission spectra of UCNP-QD (organic dyes) complex based on lumines-

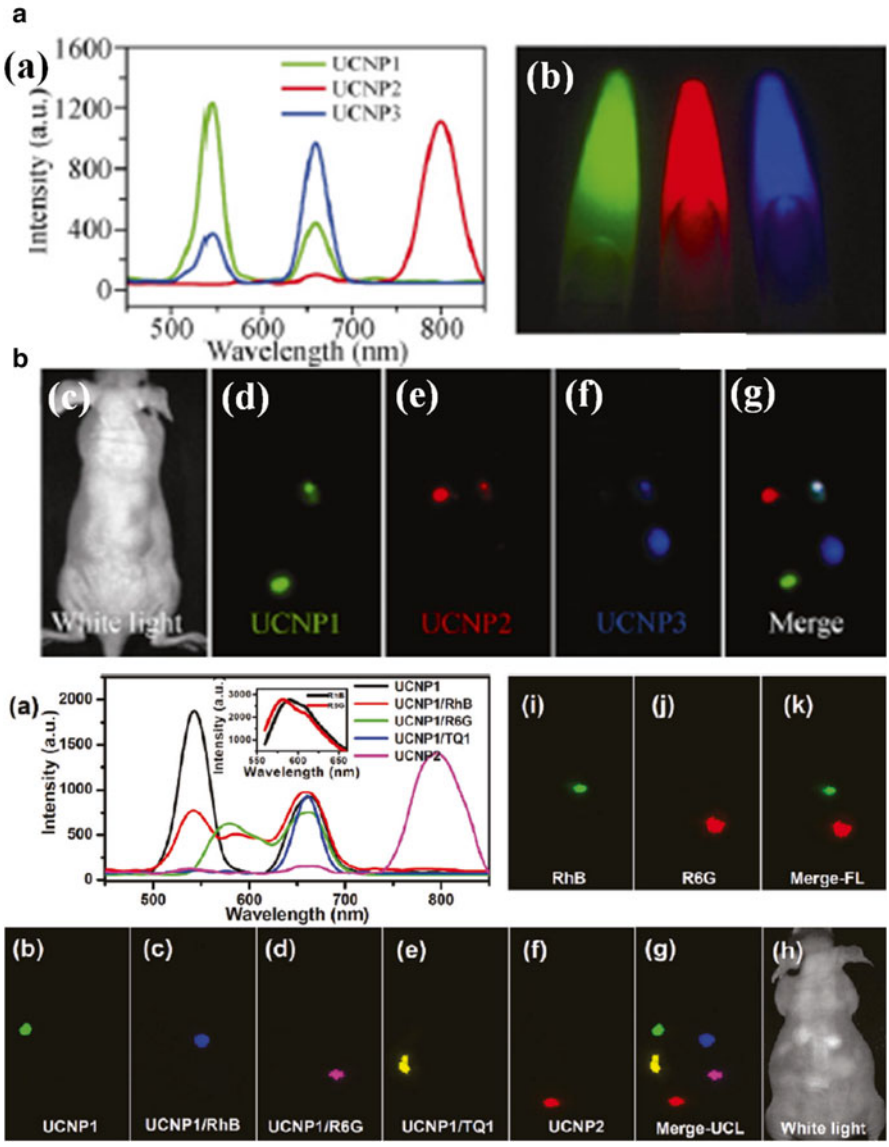

Fig. 5.1 (**a**) Multicolor UCL imaging: (*a*) UCL emission spectra of three UCNP solutions under 980 nm NIR laser excitation; (*b*) a multicolor fluorescence image of three UCNP solutions obtained by the Maestro in vivo imaging system (CRi, Inc.); (*c*) a *white light* image of a mouse subcutaneously injected with UCNPs; (*d–f*) in vivo multicolor images of a nude mouse subcutaneously injected with different UCNP solutions; (*g*) three colors of UCNPs were clearly differentiated after spectral unmixing. (**b**) Multicolor in vivo UCL imaging of LRET-tuned UCNPs in mice: (*a*) UCL emission spectra of solutions of *UCNP1*, *UCNP2*, *UCNP1/RhB*, *UCNP1/R6G*, and *UCNP1/TQ1*. Insert: down-conversion fluorescence spectra of *RhB* and *R6G* under *green light* excitation. (*b–g*) In vivo multicolor UCL images of a nude mouse subcutaneously injected with five colors of UCNP solutions after spectral unmixing. (*h*) A *white light* image of the imaged mouse. (*i–k*) In vivo multicolor down-conversion fluorescence images of the mouse under *green light* excitation ((**a**) Reprinted from Ref. [56], with kind permission from Springer Science+Business Media. (**b**) Reprinted with the permission from Ref. [9]. Copyright 2011 American Chemical Society)

cence resonance energy transfer (LRET) from UCNP core to QDs (or organic dyes). In the work by Liu et al. [9], organic dyes (RhB/R6G/TQ1) were integrated with UCNPs by hydrophobic force to make a multicolor UCL imaging probe with tunable luminescence emission based on the LRET under NIR excitation. As shown in Fig. 5.1b, by subcutaneously injecting five different UCNP solutions (UCNP1, UCNP1/RhB, UCNP1/R6G, UCNP1/TQ1, and UCNP2) into the back of nude mice, five different colors were obtained after spectral deconvolution, which clearly demonstrated the UCL imaging of different colors at their corresponding injection sites without noticeable interference (parts b–h of Fig. 5.1b). Based on the same LRET strategy, Kim's group designed the UCNP-QD complex system for multicolor imaging upon different wavelengths of light excitation [58].

5.3.1.2 UCNPs for Tracking UCL Imaging

Thanks to the extremely low autofluorescence of UCL imaging, UCNPs can be used for in vitro cell labeling as well as in vivo tracking. For example, Zhang et al. [59] used silica-coated UCNPs to dynamically track live myoblast cells in vitro and transplanted cells in a living mouse model in vivo. Then Li et al. [60] fabricated strong luminescent UCNPs (β-$NaLuF_4$: Gd/Yb/Tm) to label KB cells in vivo with high tracking sensitivity. The corresponding detection limits are 50 and 1,000 UCNP-labeled KB cells for subcutaneous and intravenous injection, respectively (Fig. 5.2a, b). Moreover, high-contrast deep-seated UCL imaging of a whole-body black mouse was also achieved with a large penetration depth of ~2 cm.

Besides cancerous cells, mesenchymal stem cells (MSCs) can be also labeled by UCNPs. In a recent study by Liu's group [61], oligoarginine-conjugated UCNPs were used for highly efficient MSC labeling and in vivo long-term tracking with ultrahigh sensitivity at nearly the single-cell level, which can hardly be achieved by other exogenous fluorescent or magnetic labeling probes. More importantly, the UCNP-based MSC labeling/tracking approach would not affect the proliferation and differentiation of MSCs over a course of 2 weeks, and as few as ten UCNP-labeled cells were successfully detected in vivo, thus demonstrating the super advantages over other stem cell labeling techniques. On this basis, they further designed multifunctional UCNPs@IONPs@Au composite (MFNPs) for in vitro labeling and in vivo tracking of MSCs by both UCL optical and MR imaging techniques, which also achieves a ultrahigh tracking sensitivity with as few as ≈ 10 cells detectable in a mouse (Fig. 5.2c, d) [62]. Under a magnetic field, MFNP-labeled MSCs after being injected into mice can be remotely controlled and magnetically targeted and delivered to the wound site for enhancing the tissue-repairing efficacy (Fig. 5.2e, f), which demonstrates a promising prospect for future magnetic/luminescent imaging-guided MSC therapy applications.

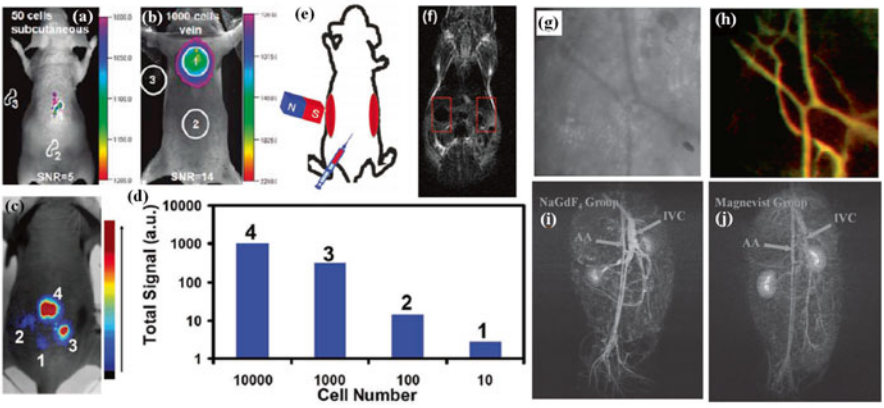

Fig. 5.2 (**a**, **b**) In vivo UCL imaging of athymic nude mice after (**a**) subcutaneous injection of 50 KB cells and (**b**) vein injection of 1,000 cells. The KB cells were incubated with 200 μgmL β-$NaLuF_4$: Gd/Yb/Tm nanoparticles for 2 h. (**c**–**f**) In vivo tracking of MFNP-labeled mMSCs: (**c**) A UCL image of a mouse subcutaneously injected with various numbers of mMSCs (≈10–10^4) labeled with MFNP-PEG. (**d**) Quantification of UCL signals. (**e**) A scheme showing that the wound-bearing mouse was anesthetized by isoflurane inhalation and i.p. injected with MFNP-labeled mMSCs. A magnet was attached to the left-side wound for 6 h before imaging. (**f**) In vivo MR image of the wound-bearing mouse. (**g**, **h**) UCL imaging of blood vessels in the mouse ear following tail vein injection of PEG-coated Y_2O_3:Yb/Er nanoparticles; (**g**) blood vessels imaged with a *blue light* filter. (**h**) UCL image with excitation at 980 nm. (**i**, **j**) MR angiography of rabbits within 3 min after injected with the **i** NaGdF4 nanodots or (**j**) Magnevist: abdominal aorta (*AA*) and inferior vena cava (*IVC*) ((**a**, **b**) Reprinted with the permission from Ref. [60]. Copyright 2011 American Chemical Society. (**c**–**f**) Reprinted with the permission from Ref. [62]. Copyright 2013 Wiley-VCH Verlag GmbH & Co. KGaA. (**g**, **h**) Reprinted with the permission from Ref. [66]. Copyright 2009 Royal Society of Chemistry. (**i**, **j**) Reprinted with the permission from Ref. [67]. Copyright 2014 Wiley-VCH Verlag GmbH & Co. KGaA)

5.3.1.3 UCNPs for Tumor-Targeted UCL Imaging

Tumor-targeted imaging plays a very important role in cancer diagnosis and the following imaging-guided positioned therapy. By the attachment of some special targeting ligands, UCNPs can be efficiently accumulated in tumors for high-contrast UCL imaging upon NIR light excitation. In 2009, Li's group firstly realized the in vivo tumor-targeting UCL imaging by using folic acid (FA)-modified UCNPs [63]. As a widely used targeting agent, FA has a high affinity for folate receptors (FR) that are overexpressed in many human cancerous cells like HeLa. Therefore, after intravenous injection of FA-modified UCNPs into HeLa tumor-bearing nude mice for 24 h, strong UCL signal appeared in the HeLa tumor region, while no UCL signal was observed in the control group (mice intravenously injected with amine-modified UCNPs), thus demonstrating excellent tumor-targeted UCL imaging. Besides FA, RGD (arginine–glycine–aspartic acid) peptide can target $\alpha_v\beta_3$-integrin receptor overexpressed tumors. In about 4 h postinjection of RGD-modified UCNPs, Li et al. observed obvious UCL signal in the U87MG tumor (expressing high levels

of integrin $\alpha_v\beta_3$) as compared to invisible signal in MCF-7 tumor (expressing low levels of integrin $\alpha_v\beta_3$) [64]. Our group also successfully used RGD-conjugated $BaYbF_5$:Tm nanoparticles for targeted UCL imaging of U87MG tumor [15]. Besides subcutaneously xenotransplanted U87MG tumors, the UCL imaging intracranial glioblastomas have been also realized by attaching a dual-targeting ligand ANG to UCNPs [65], which can efficiently cross the blood–brain barrier (BBB) and target the glioblastoma for UCL imaging diagnosis. Therefore, in order to realize highly efficient tumor-targeting UCL imaging, superior targeting ligands with strong binding affinity should be designed for the rich accumulation of UCNPs in tumors, which will be a research hotspot in the future.

5.3.1.4 UCNPs for Vascular UCL Imaging

Up to date, the early diagnosis of vascular permeability and vessel functional abnormality can help efficiently prevent the vascular diseases which have been another major threat to human health. Due to the high sensitivity and photostability without autoluminescence, UCNPs may serve as an advanced imaging tool for visualizing blood vessels in vivo. The first report of using UCNPs for vascular UCL imaging is Hilderbrand's group [66], who synthesized PEG-coated Y_2O_3:Yb/Er nanoparticles with UCL emissions centered at 660 nm for strong red luminescent blood pool imaging in vivo upon NIR irradiation. The ear blood vessel could be clearly visualized by intravenous injection of UCNPs under a whole-field-illumination upconversion microscope (Fig. 5.2g, h). Then Zhang et al. also used silica-coated UCNPs ($NaYF_4$:Yb/Er@SiO_2 nanoparticles) for the live myoblast cell tracking as well as ear blood vessel UCL imaging via tail vein injection [59]. However, as limited by the relatively low spatial resolution, luminescent imaging fails to distinguish the whole blood vessels more clearly, which can be improved by magnetic resonance (MR) imaging or other high-resolution imaging tools. For example, our group synthesized ultrasmall $NaGdF_4$ nanoparticles (with a high r_1 value of 8.93 $mM^{-1}s^{-1}$) for high-resolution blood pool MR imaging with the abdominal aorta (AA) and inferior vena cava (IVC) distinctly delineated (Fig. 5.2i, j) [67]. More importantly, the subvascular details and micrangium can be also clearly distinguished, which can contribute to the accurate diagnosis of vascular pathema or other vascular diseases.

5.3.1.5 UCNPs for Lymphatic UCL Imaging

As most cancerous cells frequently metastasize to the local lymph nodes, the identification of sentinel lymph nodes based on the lymphatic imaging is of essential importance for monitoring the tumor metastasis and guiding the surgical operation. As an excellent luminescent probe, UCNPs have been used by many researchers for high-contrast UCL imaging of lymph nodes without autofluorescence. The first use of UCNPs for lymphatic UCL imaging is Kobayashi's group [68], who directly captured the lymph node pictures without post-processing. Then Li et al. [69] and

Liu et al. [56] also successfully realized the lymphatic capillary UCL imaging of small animals with high signal to noise ratio upon relatively low power density of NIR irradiation (Fig. 5.3a, b). More interestingly, by intracutaneous injection of three different kinds of UCNPs with multicolor emission, strong multicolor UCL imaging signals appeared in the three primary lymph nodes where each color of UCNPs migrated via lymphatic drainage (Fig. 5.3a), thus demonstrating the advantages of UCNPs in multicolor lymphatic UCL imaging. However, due to the limited penetration depth of NIR irradiation, deep-seated lymph nodes can't be achieved by UCL imaging, which needs the exploration of more advanced imaging modalities, such as PET imaging with high sensitivity and unlimited penetration.

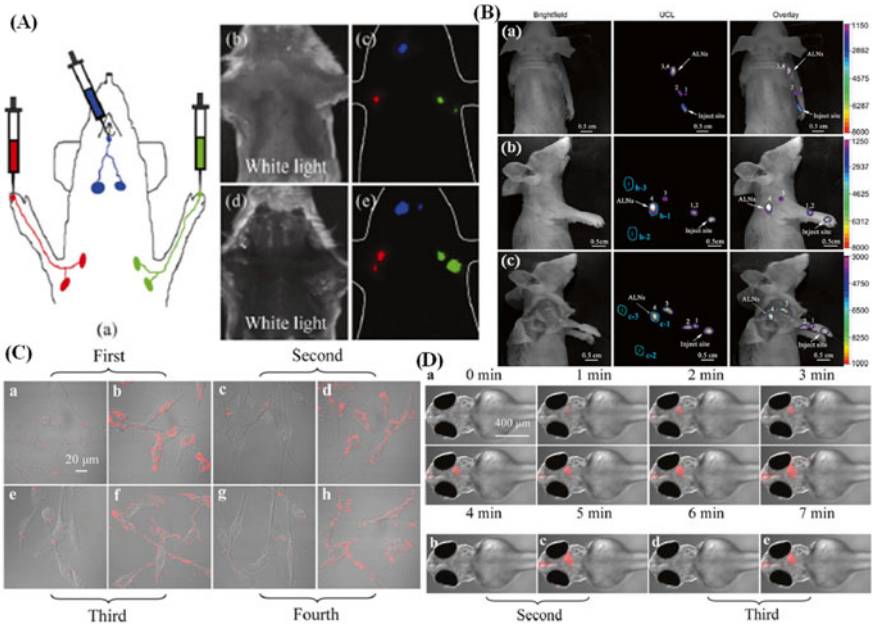

Fig. 5.3 (**a**) In vivo multiplexed lymphangiography with UCNPs: (*a*) a schematic illustration of UCNP-based lymph node mapping; (*b*) a *white light* image of a mouse injected with UCNPs; (*c*) a three-color spectrally resolved in vivo UCL image showing different UCNP colors from the corresponding lymph nodes under the skin; (*d*) a *white light* image of the same mouse after dissection; (*e*) a UCL image of the dissected mouse. (**b**) In vivo lymphatic drainage UCL imaging at 800 nm was clearly detected at four different draining lymph basins (*1*, *2*, *3*, *4*) along the right antebrachium of the nude mouse. Detection of upconversion luminescence in (*a*) prostrate or (*b*) lateral position. (*c*) The lymphatic drainage UCL imaging after removal of skin and fatty tissues. (**c**) CLSM images of U87MG cells loaded with nanosensors and exposed to cycles of normoxia (*a*, *c*, *e*, *g*) and hypoxia (*b*, *d*, *f*, *h*) conditions for 6 h. (**d**) CLSM images of living zebrafish embryos after injection of nanosensors followed by adding BDM. UCL images were obtained under the excitation at 980 nm and emission at 550–650 nm. After adding freshwater, red emission in the brain was quenched under NIR exposure ((**a**) Reprinted from Ref. [56], with kind permission from Springer Science+Business Media. (**b**) Reprinted with the permission from Ref. [69]. Copyright 2011 Elsevier B. V. (**c**, **d**) Reprinted with the permission from Ref. [71]. Copyright 2014 American Chemical Society)

5.3.1.6 UCNPs for Hypoxic UCL Imaging

As a principal signature of solid tumors, tumor hypoxia, arising from the inadequate supply of oxygen in blood vessels, has been a major cause for the treatment failure of solid tumors and the induction of tumor invasion/metastasis [70]. Luminescent imaging has been used for the accurate diagnosis of tumor hypoxia and quantitative estimation of hypoxic degree. Considering the intrinsic drawbacks (e.g., low photostability in bioreductive microenvironment, low penetration depth, etc.) of traditional oxygen probes, our group developed an ultrasensitive nanosensor by engineering UCNPs for selective hypoxic UCL imaging based on the LRET from UCNPs to oxygen indicator $[Ru(dpp)_3]^{2+}Cl_2$ under NIR irradiation [71]. Compared with free $[Ru(dpp)_3]^{2+}Cl_2$, our designed nanosensor can reversibly detect the level of hypoxia both in vitro (hypoxic U87 cells, Fig. 5.3c) and in vivo (zebrafish, Fig. 5.3d) based on the corresponding luminescence emission intensity with high sensitivity and large penetration depth. The ultrasensitive nanosensor is expected to be used for hypoxic UCL imaging of solid tumors to provide significant guidance for the subsequent therapeutic decisions.

In summary, thanks to the superior advantages over traditional luminescent probes, UCNPs can serve as an excellent UCL imaging probe for the accurate diagnosis of big diseases as well as quantitative sensing of some biological matters and tumor microenvironment (e.g., hypoxia, pH, temperature, etc.). However, in order to promote the future clinical applications of UCNPs, many aspects need to be further improved, such as the enhancement of UCNPs' quantum yield, the lowering of UCNPs' potential toxicity, and so on.

5.3.2 UCNPs for Multimodal Imaging

As the saying goes, there exists no perfect single imaging probe because each imaging modality has its intrinsic drawbacks and thus fails to reflect all the necessary imaging information. Therefore, the development of multimodal imaging probe by the combination of multiple imaging modalities into one system is of essential importance for acquiring all the imaging data and enhancing the diagnostic accuracy. By suitable doping strategy, UCNPs can be engineered as an excellent multimodal imaging probe to realize the cellular scale to whole-body level imaging with extremely high sensitivity and spatial resolution.

5.3.2.1 UCNPs for MR/UCL Bimodal Imaging

The most common UCNP-based multimodal imaging probe is the simple combination of MR/UCL by doping Gd^{3+} into the host lattice. This bimodal imaging probe possesses all the advantages of MR/UCL and provides high sensitivity for in vitro imaging as well as and high spatial resolution for in vivo imaging [8]. For example,

Li et al. synthesized PAA-coated Yb/Er/Tm/Gd co-doped UCNPs (NaGdF4:Yb/Er/Tm−PAA) for simultaneous T_1-MR imaging and NIR-NIR UCL imaging of the whole-body animals in vivo (Fig. 5.4a, b) [72]. Zhao et al. synthesized Yb/Er/Tm-doped Gd_2O_3 nanoparticles for simultaneous T_1-MR and strong multicolor UCL imaging [73]. The corresponding emission colors could be tuned by simply changing either the doping Ln^{3+} or co-dopant concentrations. Furthermore, by doping Mn^{2+} instead of Gd^{3+} into UCNPs, strong red UCL emission plus MR imaging capacities can be realized [74].

Besides incorporating Gd^{3+} into the host, the epitaxial growth of a $NaGdF_4$ layer on the surface of the $NaYF_4$ host to fabricate core/shell (multi-shell) structured UCNPs can not only improve the MR imaging contrast by significantly increasing the r_1 value but also greatly enhance the UCL imaging intensity by suppressing non-radiative decay and passivating surface defects. In order to evidence this point, our group conducted a series of comparative studies [11, 75] by fabricating various kinds of core/shell structured UCNPs or dense/mesoporous silica-coated UCNPs and comparing their r_1 value/UCL emission intensity, which provides a deep perspective for magnetic resonance (MR) sensitivity, and UCL emission intensity optimization of Gd^{3+}-doped UCNPs. Liu et al. [76] and Zhang et al. [77] have performed similar systemic studies, which all shed light on the design of optimized Gd^{3+}-doped UCNPs and speeding up the future clinical translation of the promising MR/UCL bimodal molecule imaging probes.

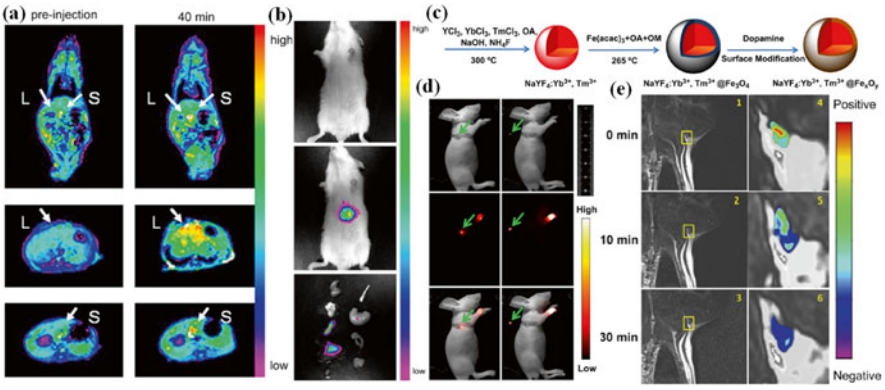

Fig. 5.4 (**a**) Color-mapped MR coronal images of the whole body and transversal cross-sectional images of the (*L*) liver and (*S*) spleen of mice at preinjection and at 40 min after intravenous injection of NaGdF4:Yb/Er/Tm−PAA. (**b**) In vivo and ex vivo UCL imaging of mouse after intravenous injection of NaGdF4:Yb/Er/Tm−PAA. (**c**) Schematic representation of the synthetic routine of the water-soluble $NaYF_4$:Yb^{3+},Tm^{3+}@Fe_xO_y nanocrystals. (**d**) Ex vivo UCL images of the lymphatic system of a nude mouse sacrificed after injection with $NaYF_4$:Yb^{3+},Tm^{3+}@Fe_xO_y nanocrystals for 40 min. *Green arrow* marked the lymphatic nodes. (**e**) MR images of the armpit region after injection with $NaYF_4$:Yb^{3+},Tm^{3+}@Fe_xO_y nanocrystals and color-mapped coronal images of lymph node at various times ((**a**, **b**) Reprinted with the permission from Ref. [72]. Copyright 2010 Elsevier B. V. (**c**–**e**) Reprinted with the permission from Ref. [79]. Copyright 2011 Elsevier B. V)

It is well known that T_1-weighted MRI contrast agents (as called positive MRI contrast agents) can change the spin–lattice/the protons of coordinated/nearby water molecules to brighten the image signals, while T_2-weighted MRI contrast agents (as called negative MRI contrast agents) can alter the spin–spin relaxation time to darken the image signals. As a representative T_2-MRI probe, Fe_3O_4 nanoparticles (SPIONs) have been widely used for darken MR imaging of human organs due to their good biocompatibility and special superparamagnetic properties. Unfortunately, black Fe_3O_4 nanoparticles could largely absorb the UCL emission and thus quench the luminescence of UCNPs, which adds to the difficulty in preparing excellent T_2-MR/UCL bimodal imaging probes.

Some groups have tried to prevent the UCL emission quenching by SPIONs through the smart design of UCNP/SPION nanocomposite. For example, in the year 2010, our group firstly developed a "neck-formation" strategy [78] to fabricate silica-shielded magnetic upconversion fluorescent oligomers (SMUFOs) by connecting SPION@SiO_2 and UCNPs@SiO_2 nanoparticles through the Si-O-Si bridges between them. Due to the high magnetic/photostability and quenchless UCL properties, the designed SUMFOs were successfully used for T_2-weighted MR and UCL bimodal imaging of Walker 256 tumor in a SD mouse. By coating a 5 nm Fe_xO_y shell on the $NaYF_4$:Yb/Tm core, Li et al. synthesized silica-free $NaYF_4$:Yb/Tm@Fe_xO_y nanocomposites which could be applied for T_2-MR/UCL bimodal imaging of the lymphatic systems in vivo (Fig. 5.4c–e) [79]. Besides, Liu et al. developed a layer-by-layer assembly approach to synthesize core/shell/shell structured nanocomposites (MFNPs) with UCNPs as the core, a thin gold layer as the outer shell, and a layer of ultrasmall SPIONs in between [80]. Thanks to the smart integration of UCNPs/SPIONs and strong NIR absorption of gold, the designed MFNPs could be used for T_2-MR/UCL bimodal imaging as well as magnetically targeted photothermal therapy in vitro and in vivo. Zhang et al. also used a facile ion exchange route to fabricate a hydrophilic rattle-structured Fe_3O_4@SiO_2@$NaYF_4$:Yb/Er nanoprobes for T_2-MR/UCL bimodal imaging as well as the antitumor drug doxorubicin (DOX)-delivered chemotherapy against H22 tumors under the enhanced magnetic targeting [81].

In order to completely eliminate the UCL quenching by SPIONs in the design of excellent T_2-MR/UCL bimodal imaging probes, the exploration of other functional ions for T_2-MR imaging is urgently needed. Fortunately, van Veggel et al. found that the paramagnetic dysprosium (Dy^{3+}) ion-doped UCNP was one of the best choices for T_2-weighted MR imaging because of its high magnetic moment (10.6 μB) and short electronic relaxation time (~0.5 ps) [82]. Moreover, these Dy^{3+}-doped UCNPs (e.g., $NaDyF_4$, $NaHoF_4$, etc.) have been found especially suitable for T_2-MR imaging in ultrahigh field (9.4 T) MRI because their corresponding r_2 relaxivity value was greatly enhanced with the increasing magnetic field, which should be explained by the Curie spin relaxation mechanism. Therefore, the van Veggel's exciting finding provides a new perspective for the design of ultrahigh field T_2-MR/UCL bimodal imaging probe with much higher spatial resolution in ultrahigh field MRI and negligible luminescence quenching.

5.3.2.2 UCNPs for UCL/MRI/CT (PET/SPECT) Trimodal Imaging

Besides MR/UCL bimodal imaging probes, recently more attentions have been paid to the construction of MRI/UCL/CT or MRI/UCL/PET trimodal imaging probes, which can greatly improve the imaging quality and enhance the diagnostic accuracy. Different from MR and UCL imaging with high sensitivity and spatial resolution, X-ray computed tomography (CT) imaging can provide high-resolution three-dimensional (3D) structure details of tissues based on their differential X-ray absorption. Therefore, the combination of MR, UCL, and CT into one system to generate a trimodal imaging probe may not only achieve high-sensitivity cellular imaging but also provide clear 3D soft tissue details. Instead of small iodinated molecules, several high-Z atom (e.g., Yb, Lu, Au, etc.)-doped/contained nanoparticles can serve as better CT contrast agents because of their stronger X-ray attenuation [83]. By the smart assembly of these CT contrast agents with the above MR/UCL bimodal imaging probes, MR/UCL/CT trimodal imaging probes are produced for concurrent trimodal imaging of malignant tumors.

The first trimodal imaging probe was designed by our group [51], who synthesized PEGylated $NaYF_4$: Yb/Er/Tm/Gd@SiO_2-Au@PEG5000 nanoparticles (UCS-Balls) by attaching ultrasmall Au nanoparticles to the surface of silica-coated Gd-UCNPs. These UCS-Balls can serve as an excellent trimodal probe for simultaneous T_1-weighted MR/NIR-vis UCL/enhanced CT imaging of Walker 256 tumors after intratumoral injection (Fig. 5.5a). In order to avoid the potential UCL signal blocking by the outer Au nanoparticles, our group further synthesized radiopaque fluorescence-transparent TaOx nanoparticles decorated upconversion nanophosphors (UCNLs) for high-intensity/contrast CT/MRI/UCL trimodal imaging in vitro and in vivo without detectable mutual imaging interference among the three modalities [12]. Besides, with the help of the strong X-ray attenuation characteristics of Gd/Yb elements and good biocompatibility of PEG, the long-circulating trimodal imaging probe PEGylated Gd_2O_3:Yb^{3+} /Er^{3+} nanorods were synthesized by Qu's group through a facile and large-scale hydrothermal approach, which could provide detailed and complementary information from T_1-MR/UCL/CT trimodal imaging [84]. Thanks to the high atomic number of Lu, Li et al. [85] even developed Gd^{3+} complex-modified $NaLuF_4$-based UCNPs for efficient trimodal imaging of the whole body of mice with high T_1-MRI enhancement, bright NIR-to-NIR UCL emissions, and excellent X-ray absorption.

Besides T_1-MR/UCL/CT trimodal imaging probes, T_2-MR/UCL/CT probes were also designed by Li et al. [86], who synthesized core/shell structured Fe_3O_4@$NaLuF_4$:Yb/Er/Tm nanoparticles (MUCNP) [86] by a stepwise method to realize T_2-MRI/UCL/CT trimodal imaging of cancerous cells in vitro and tumor tissues in vivo (Fig. 5.5b). Very recently, our group developed a novel T_2-MR/UCL/CT trimodal imaging probe by exploring the T_2-weignted contrast properties of Ho^{3+} to replace black Fe_3O_4, which can completely solve the luminescent emission quenching problem and even enhance the UCL intensity [87]. Unlike other composite nanostructures, the single Ho^{3+}-doped UCNPs ($NaYbF_4$:Ho) were synthesized by a simple one-pot thermal decomposition method for win–win multimodal T_2-MRI/

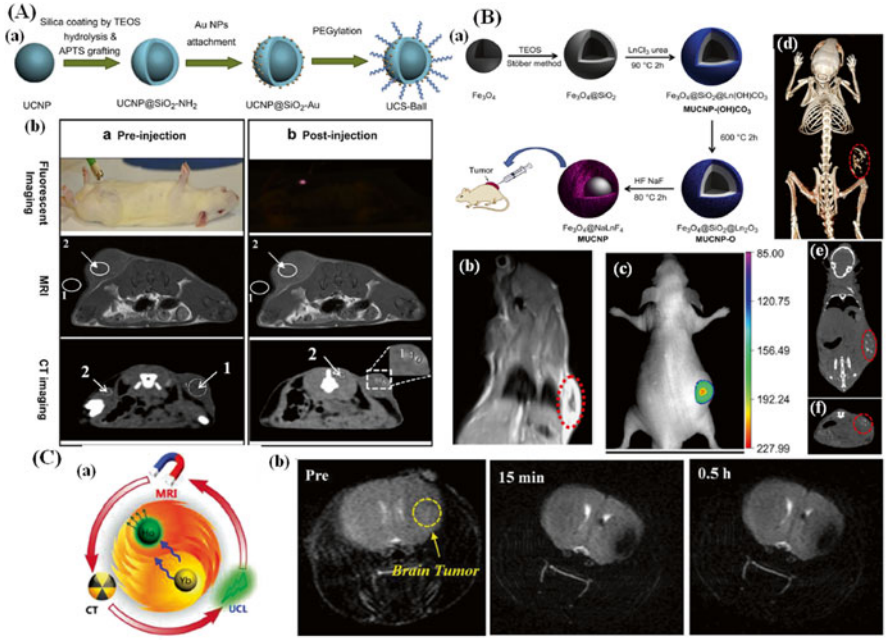

Fig. 5.5 (**a**) (*a*) Schematic illustration for the synthesis of UCS-Balls. (*b*) Trimodal images of mice bearing a Walker 256 tumor using UCS-Balls: preinjection (*left*), postinjection (*right*). (**b**) (*a*) Schematic representation of the synthetic routine of the multifunctional Fe_3O_4@$NaLuF_4$:Yb/Er/Tm nanoparticle (MUCNP). (*b*) T_2-weighted coronal images of the nude mice bearing a tumor after intratumoral injection of MUCNP. (*c*) In vivo UCL images of the tumor-bearing nude mice. (*d–f*) In vivo (*d*) CT volume-rendered and maximum intensity projection of (*e*) coronal, (*f*) transversal images of the tumor-bearing mouse. (**c**) (*a*) Schematic diagram of Ho^{3+}-doped UCNPs as the T_2-MR/UCL/CT multimodal imaging. (*b*) In vivo T_2-MR imaging of glioblastoma-bearing mice before and at various time points after intravenous injection of Ho^{3+}-doped UCNPs ((**a**) Reprinted with the permission from Ref. [51]. Copyright 2012 Elsevier B. V. (**b**) Reprinted with the permission from Ref. [86]. Copyright 2012 Elsevier B. V. (**c**) Reprinted with the permission from Ref. [87]. Copyright 2014 Wiley-VCH Verlag GmbH & Co. KGaA)

UCL/CT imaging of the whole mouse body without luminescence quenching. More importantly, the Ho^{3+}-doped UCNPs could be also used for the efficient T_2-weighted MR imaging of glioblastoma by overcoming the difficulty in the clinical diagnosis of brain tumors (Fig. 5.5c).

As another noninvasive radioactive imaging modality, PET/SPECT has been used for the whole-body imaging and quantitative biodistribution estimation due to its extremely high detection intensity. Especially, PET imaging is very suitable for the lymphatic imaging and accurate localization of lymph node by overcoming the drawbacks of traditional luminescent imaging, such as autofluorescence from biological sample, low signal to noise ratio (SNR), and so on. Recently, some radionuclides have been used for PET imaging. For example, by incorporating ^{18}F into the UCNP lattice, Li's group [16] developed ^{18}F-labeled $NaYF_4$:Yb/Tm nanoparticles

with an average yield of more than 90 % for the high-sensitivity PET imaging of whole-body small animals and lymphatic monitoring (Fig. 5.6a, b). Meanwhile, the ^{18}F-doped UCNPs could be also real-time tracked in vivo for biodistribution analysis. However, due to the extremely short half-life ($t_{1/2}$, 1.829 h) of ^{18}F that may seriously limit its biological applications in long-term imaging, the same group embedded ^{153}Sm into $NaLuF_4$:Yb/Tm nanoparticles to replace ^{18}F by a one-pot hydrothermal synthetic method [19]. Thanks to the much longer half-life (46.3 h) of ^{153}Sm and emission of medium-energy beta rays, the synthesized $NaLuF_4$:^{153}Sm/Yb/Tm nanoparticles could be used for long-term SPECT imaging (Fig. 5.6c–g) for in vivo quantitative distribution monitoring of the nanomaterials. Certainly, there are other long-term radionuclides that remain to be explored/applied for PET/SPECT imaging, such as ^{64}Cu ($t_{1/2}$, 12.7 h), ^{86}Y ($t_{1/2}$, 14.7 h), ^{124}I ($t_{1/2}$, 4.2d), and so on.

By the co-doping of Gd^{3+}/Yb^{3+}/Er^{3+} into ^{18}F-labeled UCNPs (^{18}F-labeled $NaYF_4$:Gd/Yb/Er nanoparticles), Li et al. successfully fabricate a novel MR/UCL/PET trimodal imaging probe for high-sensitivity/solution imaging from the cellular scale to whole-body evaluation by integrating the advantages of these three imaging modalities [88]. Specially, PET imaging can realize the whole-body imaging with high detection sensitivity as well as reach below the picomolar range for functional imaging. The in vivo MR and ex vivo UCL imaging can provide the complementary information including the cellular-level observation. So the combination of MR/UCL/PET imaging modalities within the trimodal probe is of great value for the future accurate diagnostic applications in clinic.

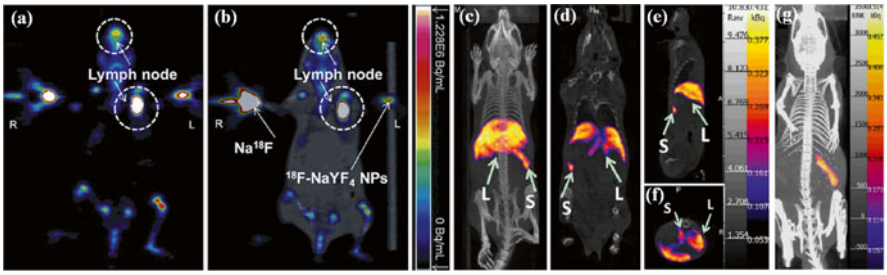

Fig. 5.6 (**a**) PET imaging and (**b**) PET/CT imaging of lymph node 30 min after subcutaneous injection of ^{18}F-UCNPs. ^{18}F-UCNPs into the left paw footpad, signal in lymph node reached the peak intensity and maintained it to 60 min postinjection. While as control-free $^{18}F^-$ ions injected into the right paw showed no lymphatic imaging ability. (**c**–**g**) In vivo SPECT images after intravenous injection of Sm-UCNPs. (**c**) Whole-body three-dimensional projection, (**d**) coronal, (**e**) sagittal, and (**f**) transversal images acquired at 1 h and (**g**) whole-body three-dimensional projection images acquired at 24 h are shown, respectively. The *arrows inset* point to the liver (*L*) and spleen (*S*) ((**a**, **b**) Reprinted with the permission from Ref. [16]. Copyright 2011 Elsevier B. V. (**c**–**g**) Reprinted with the permission from Ref. [19]. Copyright 2013 Elsevier B. V)

5.3.2.3 UCNPs for UCL/MRI/CT/SPECT Four-Modal Imaging

In order to further enhance the diagnostic accuracy, the integration of all the above four imaging modalities (MR/UCL/CT/SPECT) into one system for generating a four-modal imaging probe may be an ideal strategy. Very recently, Li's group [18] synthesized core/shell structured $NaLuF_4$:Yb,Tm@$NaGdF_4$-(^{153}Sm) nanoparticles by the epitaxial growth of a 4 nm $^{153}Sm^{3+}$-doped $NaGdF_4$ shell on the $NaLuF_4$:Yb/Tm core (Fig. 5.7a, b), which resulted in a novel excellent MR/UCL/CT/SPECT four-modal probe for high-quality tumor angiogenesis imaging. Due to the multiple functional ions (Lu^{3+}, Yb^{3+}, Tm^{3+}, Gd^{3+}, $^{153}Sm^{3+}$) co-doping, the $NaLuF_4$:Yb,Tm@$NaGdF_4$-(^{153}Sm) nanoparticles possess the multifunctional properties of enhanced UCL emission, excellent X-ray attenuation, relatively high r_1 value, and gamma photon emissive radioactivity. Meanwhile, the corresponding imaging results (Fig. 5.7c–h) confirmed that the designed four-modal probe could be effectively applicable for simultaneously enhanced UCL imaging, X-ray computed tomography (CT), magnetic resonance imaging, and single-photon emission computed tomography (SPECT) in vivo. It is worth mentioning that such a four-modal imaging probe may be expected to shed light on the fabrication of multifunctional nanoprobes for future bio-imaging applications by acquiring more comprehensive and accurate imaging information.

Despite the rapid progress in the development of UCNP-based multimodal imaging probes, there is still a long way to go to apply these bioprobes for clinical diagnostic applications. Firstly, more potential toxicity and biosafety of these probes should be thoroughly evaluated to ensure their biocompatibility. Secondly, suitable surface engineering should be adopted to prevent their uptake by the RES system. Thirdly, the exploitation of multimodal imaging equipment should also be speeded up to realize the concurrent multimodal in one machine. In all, we hope the UCNP-based multimodal probes will be actually applied for the early accurate diagnosis of human diseases in the near future.

5.4 Engineering UCNPs for Imaging-Guided Synergetic Therapy

Beyond applications in multimodal biomedical imaging, UCNPs can be further expanded to be used for imaging-guided therapy. By mesoporous silica coating, UCNPs can serve as delivery vehicles of anticancer drugs/radiosensitizers/photosensitizers for chemotherapy, radiotherapy, and photodynamic therapy (PDT). In clinic, only single treatment can't eradicate malignant tumors due to its intrinsic drawbacks, so the integration of different therapeutic modalities into UCNP-based theranostic system may help lead to the optimal treatment efficacy as well as realize our dream of thorough tumor elimination.

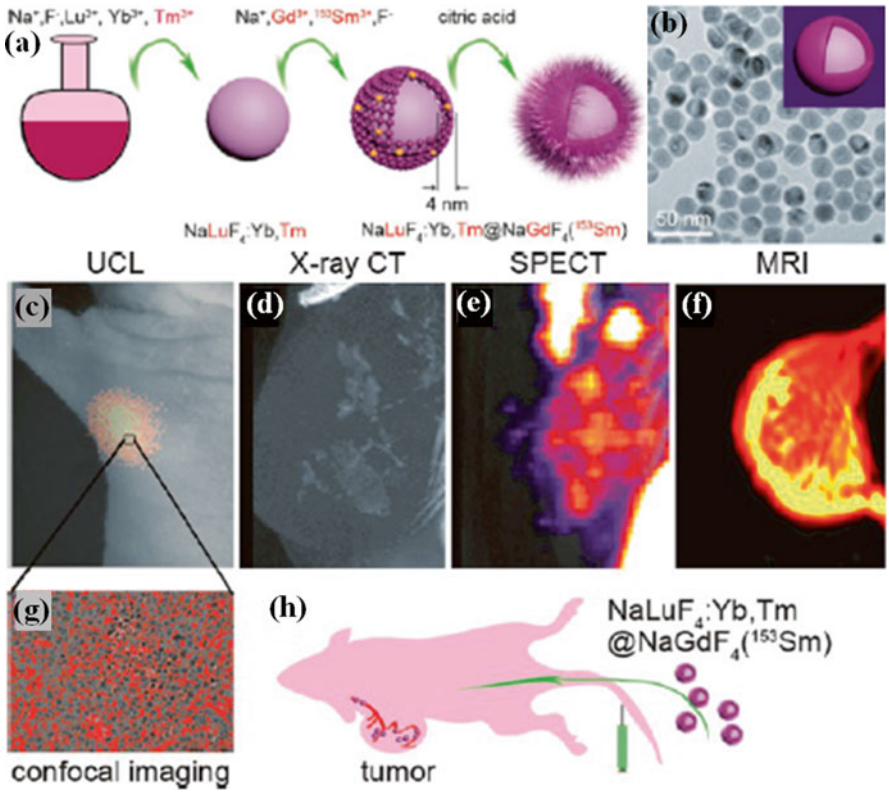

Fig. 5.7 (**a**) Schematic illustration of synthetic routine of the core/shell nanocomposite $NaLuF_4$:Yb/Tm@$NaGdF_4(^{153}Sm)$. (**b**) TEM image $NaLuF_4$:Yb/Tm@$NaGdF_4(^{153}Sm)$. (**c**–**f**) Four-modal imaging of the focused tumor from the tumor-bearing nude mouse 1 h after intravenous injection of $NaLuF_4$:Yb/Tm@$NaGdF_4(^{153}Sm)$. (**c**) In vivo UCL image, (**d**) X-ray CT image, **e** SPECT image, (**f**) MR imaging of tumor. (**g**) UCL confocal image of the paraffin section of tumor tissue. (**h**) Schematic illustration of tumor angiogenesis imaging using $NaLuF_4$:Yb/Tm@ $NaGdF_4(^{153}Sm)$ as the probe (Reprinted with the permission from Ref. [18]. Copyright 2013 American Chemical Society)

5.4.1 UCNPs for PDT

As a noninvasive light-triggered treatment tool, PDT has been widely used for cancer therapy by producing cytotoxic reactive oxygen species (ROS) to kill cancerous cells. However, traditional PDT strategy of using UV or visible light to excite photosensitizers fails to treat those deep-seated tumors due to the limited penetration depth, which remains a big challenge to be overcome. Thanks to the unique feature of UCNPs in the conversion of NIR light to UV/vis light, a great deal of singlet oxygen ($^1O_2$) can be generated upon NIR irradiation based on the fluorescence resonance energy transfer (FRET) from UCNPs to photosensitizers. More importantly, by the targeted delivery of UCNPs, photosensitizers, especially those hydrophobic

ones, can be transported to tumor tissues for the further improved NIR-triggered PDT effects.

The first realization of NIR-triggered PDT is by Zhang's group [89], who coated a merocyanine-540-doped silica shell on UCNPs. Upon NIR light irradiation, merocyanine-540 could efficiently absorb the visible light emission from UCNPs to generate $^1O_2$ on killing MCF-7/AZ bladder cancerous cells. By aid of a water-in-oil reverse microemulsion strategy, Zheng's group [90] successfully synthesized UCNPs@SiO_2 nanoparticles with photosensitizer AlC_4Pc covalently incorporated into the dense silica shells, which could improve the PDT effects by enhancing the loading efficacy and avoiding the leakage of photosensitizers. Based on the same method, our group [91] prepared a new kind of sub-50 nm UCNPs@SiO_2(MB) PDT drug. In this study, we firstly focused on the control of various parameters (e.g., MB concentration, reaction time, silica shell thickness, etc.) for the inhibition of MB dimerization as well as the excellent spectral overlap between UCNP emission and MB absorption for the realization of ever higher FRET efficiency. Although the above photosensitizers loaded into the nonporous dense silica could be protected from the surrounding intricate environment, the diffusion of oxygen molecules and release of ROS are extremely limited, thus resulting in the lowering PDT efficacy to some extent. To overcome this drawback, the following effective loading strategies have been adopted for combining photosensitizer with UCNPs.

By loading photosensitizers into the mesoporous silica instead of dense silica, more oxygen molecules are diffused to "contact" UCNPs/photosensitizers and thus involved in the PDT reaction for generating much more $^1O_2$. Zhang et al. [25] firstly incorporated photosensitizers ZnPc into the mesoporous silica-coated UCNPs, which led to the continuous production of $^1O_2$ for causing significant cancerous cell death upon NIR irradiation. Unlike the above physical encapsulation of hydrophilic photosensitizers, the covalent grafting method was used for the loading of hydrophobic ones by avoiding premature leakage. For example, in a recent report by Yan et al. [92], hydrophobic photosensitizers (SPCD/HP) were covalently bonded to mesoporous silica channels to improve their solubility/stability in cell microenvironment. Meanwhile, the mesoporous silica also created the conditions for faster release of $^1O_2$ into the surrounding tumor regions. Upon NIR irradiation, the photosensitizers could absorb green/red luminescence emission from UCNPs to generate a great deal of $^1O_2$ to efficiently killing many tumor cells. Instead of covalently incorporating photosensitizers into the mesoporous silica by Si-O-Si bonds, Zhang et al. [93] developed another covalent bonding strategy to directly link rose bengal (RB) onto the surface of UCNPs. They found this covalent linking strategy could improve both the loading capacity of RB and FRET efficiency from UCNPs to RB, thus leading to the greatly elevated PDT effects. Moreover, by the attachment of targeting ligand FA (folic acid), the FA-conjugated UCNPs/RB could realize the targeted PDT by killing much more FR (folate receptor) positive JAR carcinoma cells than FR negative NIJ 3T3 cells upon 980 nm irradiation (Fig. 5.8a). Certainly, with the development of nanochemistry and nanotechnology, more effective targeted UCNP-photosensitizer drugs will be designed and applied for PDT in the near future.

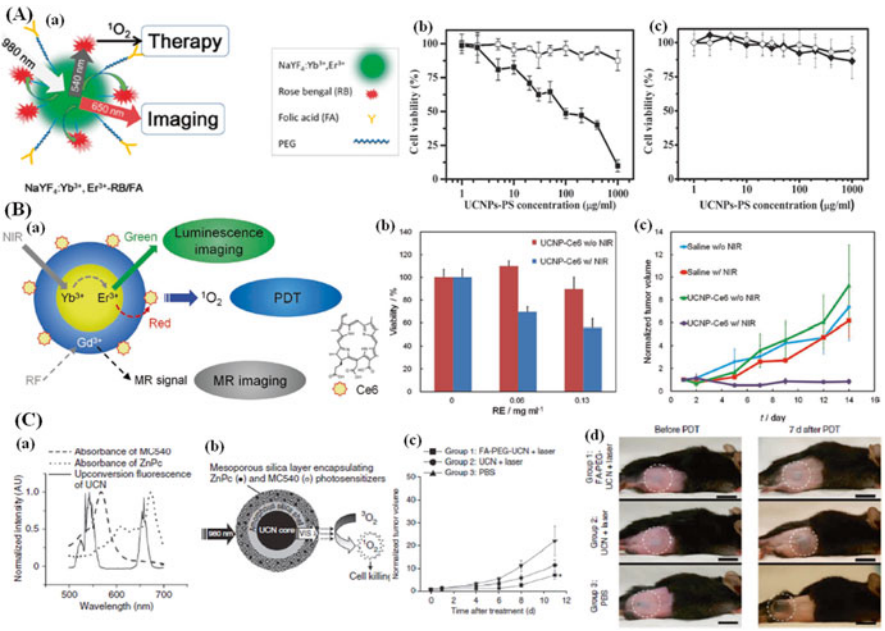

Fig. 5.8 (**a**) (*a*) Covalent conjugation of NaYF4:Yb3t,Er3t UCNPs, photosensitizer RB, and target molecule FA. (*b*, *c*) Viability of JAR cells (*b*) and NIH 3T3 fibroblasts (*c*) treated with FA-UCNPs/RB of different concentrations with (*solid*) or without (*open*) 980 nm exposure. (**b**) (*a*) Schematic illustration of dual-modal imaging and PDT using UCNP–Ce6. (*b*) Cell viability of U87MG cells incubated with UCNP–Ce6, with or without exposure to 980 nm laser. (*c*) Growth of tumors after treatments. (**c**) (*a*) The fluorescence emission spectrum of the UCN under 980 nm NIR laser excitation and the absorption spectra of ZnPc and MC540. (*b*) Schematic of mesoporous silica-coated UCNs co-loaded with ZnPc and MC540 for PDT. (*c*) Change in tumor size as a function of time after treatment to assess the effectiveness of UCN-based mediated targeted PDT in tumor-bearing mice intravenously injected with FA-PEG-UCNs. (*d*) Representative gross photos of a mouse from groups 1–3 intravenously injected with FA-PEG-UCNs, unmodified UCNs, or PBS showing the change in tumor size (highlighted by *dashed white circles*) before (0 d) and 7 d after PDT treatment ((**a**) Reprinted with the permission from Ref. [93]. Copyright 2012 American Chemical Society. (**b**) Reprinted with the permission from Ref. [94]. Copyright 2012 Wiley-VCH Verlag GmbH & Co. KGaA. (**c**) Reprinted with the permission from Ref. [95]. Copyright 2012 Nature Publishing Group)

Unlike the above PDT-related researches that mainly focus on the in vitro PDT, the following in vivo PDT studies may be more exciting and closer to future clinical cancer therapy. In 2011, Liu et al. [26] firstly performed UCNP-based PDT on tumor-bearing mice. In his study, the photosensitizer Ce6 was adsorbed onto PEGylated UCNPs to form a new UCNPs-Ce6 PDT agent, which could induce significant cancerous cell death by producing $^1O_2$ upon NIR irradiation. After injecting the UCNPs-Ce6 agent into $4T_1$ tumors grown on balb/c mice, about 70 % of tumors were completely eradicated for even without regrowth within the next 2 months by exposure to NIR light. So the mice after PDT treatment had much longer survival lifetime than the non-treated mice. Furthermore, they also evaluated the potential use of UCNP-based PDT on treating deep-seated tumors. By comparison

with the direct excitation of Ce6 using visible light, the NIR-triggered PDT using UCNPs-Ce6 demonstrated a much deeper tissue penetration depth and thus exhibited great potential in the future therapy of large or internal tumors. By the appropriate structural optimization, Hyeon et al. [94] synthesized UCNPs-Ce6 nanocomplex via both physical adsorption and covalent conjugation for in vivo MR/UCL bimodal imaging-guided PDT via intravenous injection. On the one hand, there appeared strong MR/UCL imaging signal in tumors, which evidenced that UCNPs-Ce6 nanocomplex was successfully accumulated in tumors owing to the enhanced permeability and retention (EPR) effect. On the other hand, the tumor growth was remarkably inhibited upon NIR irradiation due to the improved PDT effects (Fig. 5.8b). This study may shed on the design of high-performance UCNP-based PDT agents by accurate imaging-guided photodynamic therapy.

In order to further enhance the PDT efficacy, the excitation of two or more kinds of photosensitizers using a single-wavelength light may be a desirable strategy. In a recent report by Zhang's group [95], two photosensitizers (ZnPc and M540) whose absorption peaks overlapped with the two emission (red and green) peaks of UCNPs were simultaneously loaded into the mesoporous silica-coated UCNPs. Compared with single photosensitizer-loaded UCNPs, the ZnPc/M540 co-loaded UCNPs demonstrated substantially enhanced PDT efficacy by the greatly elevated generation of $^1O_2$ for significantly reduced tumor cell viability upon NIR irradiation. More interestingly, by the conjugation of targeting ligand FA to ZnPc/M540 co-loaded UCNPs, the in vivo targeted PDT was firstly realized in animal experiments, which showed remarkable tumor growth delay (Fig. 5.8c). In all, this study is the first example of using UCNPs for in vivo targeted PDT, which may greatly promote the exploration of other targeted UCNP-based PDT agents for future NIR-triggered therapeutic applications.

5.4.2 UCNPs for Radiotherapy

As another noninvasive treatment tool, radiotherapy has achieved great success in relieving tumor patients of pain by applying high-energy X-rays or γ-rays radiation to damage the DNA of cancerous cells [96]. Besides, by focusing all radiation precisely on tumors, radiotherapy has been used for site-specific cancer therapy with relatively low adverse effects on surrounding normal tissues. Unfortunately, most hypoxic solid tumors often develop resistance to radiation and cause the treatment failure of radiotherapy [97]. Therefore, in order to eradicate solid tumors, some radiosensitizers (radiation sensitizers) should be used to enhance the radiotherapy efficacy on killing hypoxic tumors. Based on the Compton scattering effects, some high-Z metallic nanoparticles (e.g., Au, Pt, etc.) can decompose a beam of X-rays into several beams of X-rays [98], thus greatly enlarging the X-ray radiation doses on malignant tumors and causing large-scale localized DNA damage/cell apoptosis. Therefore, by doping high-Z metal ions into the UCNP lattice, both CT contrast imaging and radiation enhancement can be realized, which will lead to the CT imaging-guided radiosensitization for enhanced diagnostic/therapeutic efficacy.

Our group is the first one to introduce high-Z ion-doped UCNPs into the fields of CT imaging-guided radiotherapy. In our study [15], $BaYbF_5$:Er nanocubes (UCA) were synthesized by a hydrothermal method with high dispersity and stability. Due to the co-doping of high-Z ions Ba^{2+} and Yb^{3+}, CT contrast imaging and radiosensitization were simultaneously realized. Finally, by the conjugation of active tumor-targeting ligand RGD, UCA-RGD nanocubes were efficiently accumulated in U87 tumors for CT imaging and enhanced radiotherapy by amplifying X-ray radiation doses due to the Compton scattering effects (Fig. 5.9). The corresponding in vivo therapy results (Fig. 5.9c) clearly showed that the combination of UCA-RGD and radiotherapy led to more significantly tumor growth delay than radiotherapy alone due to the radiosensitizing effects of high-Z ions Ba^{2+} and Yb^{3+}. Therefore, the designed UCA-RGD may be potentially developed into the next generation of targeted imaging-guided radiosensitive drugs.

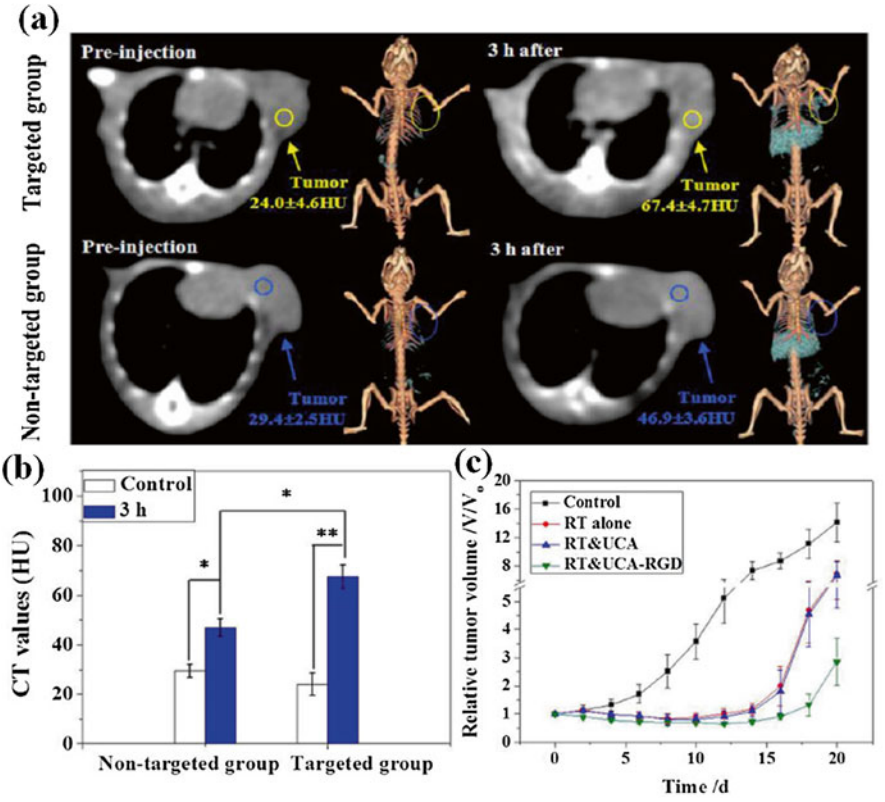

Fig. 5.9 (**a**) In vivo transverse slices and 3D volume rendering CT images of U87MG tumor-bearing mice at preinjection and 3 h after intravenous injection of UCA-RGD (targeted group) or UCA (nontargeted group). (**b**) The corresponding CT value changes in the tumor. (**c**) Growth of U87MG tumors from different groups after various treatments ($n=6$) (Reprinted with the permission from Ref. [15]. Copyright 2013 Nature Publishing Group)

5.4.3 UCNPs for Synergetic Therapy

So far, chemotherapy, radiotherapy, and PDT have become the major treatments for clinical cancer therapy, but they all have intrinsic drawbacks. For example, chemotherapy may cause systemic toxic side effects by using large amounts of free anticancer drugs. Radiotherapy and PDT are too dependent on oxygen to eradicate most hypoxic solid tumors. Therefore, in order to achieve the optimal treatment efficacy, the combinational use of the three treatments by integrating their respective superiorities may be a desirable strategy. Fortunately, by means of smart structural design, two or three therapeutic modalities can be integrated in one system to cooperate with each other to produce superadditive therapeutic effects that are greater than the theoretically projected sum. Recently, our group and other researchers have tried to engineer UCNPs for multimodal synergetic therapy.

In 2013, Zhao's group [99] co-encapsulated drugs (DOX) and photosensitizers (Ce6) onto the surface of UCNPs for synergetic chemo-/photodynamic therapy upon NIR irradiation (Fig. 5.10a). It was found that Ce6 showed negligible leakage in acidic environment and enhanced PDT efficacy based on the high FRET efficiency, while DOX was rapidly released in low pH for enhanced chemotherapy efficacy. Therefore, the in vitro therapy results (Fig. 5.10b) showed that Ce6/DOX co-loaded UCNPs killed much more cancerous cells upon NIR irradiation than any single treatment due to the cooperative interactions between chemotherapy and PDT.

Besides high-Z metallic nanoparticles, some anticancer drugs (e.g., CDDP, Dtxl, 5-Fu, etc.) could be also used as radiosensitizers for radiation enhancement effects. Recently, our group firstly designed rattle-structured UCNPs/silica nanotheranostics (UCSNs) for synergetic chemo-/radiotherapy by the encapsulation radiosensitive drugs CDDP upon X-ray irradiation (Fig. 5.10c) [100]. The corresponding in vitro and in vivo therapy results showed that CDDP-loaded UCSNs demonstrated much stronger radiation enhancement effects than free CDDP upon X-ray irradiation by killing more cancerous cells as well as causing more remarkable tumor growth delay (Fig. 5.10d). By the conjugation of targeting ligand FA to UCSNs, in vivo tumor-targeted imaging-guided synergetic chemo-/radiotherapy could be realized, which demonstrated much strong radiation enhancement effects than free CDDP (Fig. 5.10e).

In order to realize the goal of thorough tumor elimination, the above three therapeutic modalities should be simultaneously used in combination. More importantly, there exist cooperative interactions among the three treatments. For example, X-ray radiation could not only directly break down the DNA but also improve the sensitivity of cancerous cells to drugs and ROS, which thus resulted in the permanent DNA damage and cell death by imposing chemo-/photodynamic therapy. In our latest report [101], radiosensitive drugs Dtxl and radio-/photosensitizer HP (hematoporphyrin) were simultaneously loaded into the cavity and mesoporous shells of rattle-structured UCNP core/mesoporous silica nanotheranostics for synergetic chemo-/radio-/photodynamic therapy upon NIR/X-ray irradiation. It was found that the

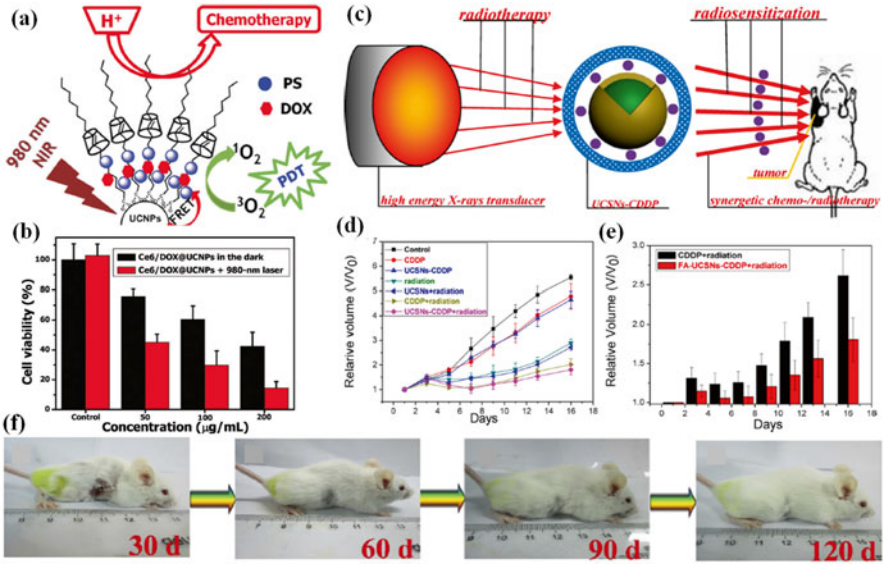

Fig. 5.10 (**a**) Scheme illustration of the combined therapeutic system for chemotherapy and PDT treatment by co-loading Ce6/DOX onto UCNPs. (**b**) Cell viabilities of A-549 cells treated with Ce6/DOX@UCNP complex (980 nm laser density, 1 W/cm^2; irradiation time, 5 min). (**c**) Schematic illustration of radiosensitization by UCSNs-CDDP. (**d**) Tumor growth curves of HeLa tumor xenografts following the different treatment in different modes; (**e**) comparison between relative volumes of HeLa tumor xenografts treated with FA-UCSNs-CDDP + radiation and CDDP + radiation. Mice were intravenously injected with FA-UCSNs-CDDP and free CDDP, respectively. (**f**) Digital photos of mice at 30, 60, 90, and 120 days after the treatment of synergetic chemo-/radio-/photodynamic therapy ((**a**, **b**) Reprinted with the permission from Ref. [99]. Copyright 2013 Wiley-VCH Verlag GmbH & Co. KGaA. (**c**–**e**) Reprinted with the permission from Ref. [100]. Copyright 2013 American Chemical Society. (**f**) Reprinted with the permission from Ref. [101]. Copyright 2014 Elsevier B. V)

tumors treated by the synergetic trimodal therapy were completely eliminated without regrowth during the next 120 days (Fig. 5.10f). We hope this study will provide a simple and useful strategy for future highly efficient oncotherapy by thorough tumor eradication. Certainly, many improvements are needed to put this technique into practice.

5.5 Summary and Outlook

In conclusion, we have summarized the latest developments in the engineering of UCNPs for multimodal biomedical imaging-guided synergetic therapy. Several effective surface modification methods have been introduced to transfer hydrophobic UCNPs into water phase for future biomedical applications. By the selective doping of different functional ions (e.g., Yb^{3+}, Gd^{3+}, Er^{3+}, $^{153}Sm^{3+}$, etc.), multimodal

biomedical imaging (MR/UCL/CT/PET) can be realized to provide superior advantages in accurate/comprehensive cancer diagnosis. As well, multimodal synergetic therapy can be achieved for highly efficient cancer treatment by the co-encapsulation of various drugs/photosensitizers/radiosensitizers into UCNP-based nanotheranostics. Therefore, UCNPs are expected to be developed into the novel intelligent nanotheranostic medicine for multimodal biomedical imaging and synergetic therapy. However, many aspects about UCNPs need to be greatly improved before going into future clinical applications.

Firstly, the quantum yield of UCNPs is very low (about 0.35 %), which inevitably results in the quite low UCL emission intensity and PDT efficacy. Therefore, more attentions should be paid to the enhancement of QY by exploring other better host matrix to fabricate much brighter UCNPs.

Secondly, similar to other inorganic materials, the potential long-term toxicity of UCNPs is a serious problem. Although the current in vitro/in vivo studies demonstrate negligible toxicity and good biocompatibility of UCNPs, the long-term in vivo chronic toxicity remains unknown and should be systemically observed. In addition, more effective surface modification strategies should be explored to further improve the biocompatibility of UCNPs.

Thirdly, in order to promote the future use of UCNPs for the in vitro/in vivo tracking and whole-body UCL imaging, the exploration of commercial imaging instruments for UCNPs with 980 nm laser module is extremely in need and should be accelerated.

Fourthly, the relative low tumor-targeting efficiency has become a big obstacle in the further improvement of the theranostic effects of UCNPs. Consequently, more effective strategies (e.g., structural optimization, surface modification, attachment of tumor-specific targeting ligands, etc.) should be developed to enhance the accumulation of UCNPs in tumors by passive/active targeting.

Last but not the least, for the realization of real-time monitoring of the therapeutic progress as well as the optimized theranostic efficacy, it is of significant importance to develop “intelligent” multifunctional nanotheranostics by the smart engineering of UCNPs. Certainly, there is still a long way to go for the true translational applications of UCNPs.

References

1. Shen J, Zhao L, Han G (2012) Lanthanide-doped upconverting luminescent nanoparticle platforms for optical imaging-guided drug delivery and therapy. Adv Drug Deliv Rev 66(5):744–755. doi:10.1016/j.addr.2012.05.007
2. Chen G, Qiu H, Prasad PN, Chen X (2014) Upconversion nanoparticles: design, nanochemistry, and applications in theranostics. Chem Rev 114(10):5161–5214. doi:10.1021/cr400425h
3. He GS, Markowicz PP, Tzu-Chau Lin, Prasad PN (2002) Observation of stimulated emission by direct three-photon excitation. Nature 415:767–770
4. Gu Z, Yan L, Tian G, Li S, Chai Z, Zhao Y (2013) Recent advances in design and fabrication of upconversion nanoparticles and their safe theranostic applications. Adv Mater 25(28):3758–3779. doi:10.1002/adma.201301197

5. Feng W, Han C, Li F (2013) Upconversion-nanophosphor-based functional nanocomposites. Adv Mater 25(37):5287–5303. doi:10.1002/adma.201301946
6. Liu Y, Tu D, Zhu H, Chen X (2013) Lanthanide-doped luminescent nanoprobes: controlled synthesis, optical spectroscopy, and bioapplications. Chem Soc Rev 42(16):6924–6958. doi:10.1039/c3cs60060b
7. Chen G, Yang C, Prasad PN (2013) Nanophotonics and nanochemistry: controlling the excitation dynamics for frequency up- and down-conversion in lanthanide-doped nanoparticles. Acc Chem Res 46(7):1474–1486
8. Zhou J, Liu Z, Li F (2012) Upconversion nanophosphors for small-animal imaging. Chem Soc Rev 41(3):1323–1349. doi:10.1039/c1cs15187h
9. Cheng L, Yang K, Shao M, Lee S-T, Liu Z (2011) Multicolor in vivo imaging of upconversion nanoparticles with emissions tuned by luminescence resonance energy transfer. J Phys Chem C 115(6):2686–2692. doi:10.1021/jp111006z
10. Wang F, Liu X (2008) Upconversion multicolor fine-tuning: visible to near-infrared emission from lanthanide-doped $NaYF_4$ nanoparticles. J Am Chem Soc 130:5642–5643
11. Chen F, Bu W, Zhang S, Liu J, Fan W, Zhou L, Peng W, Shi J (2013) Gd3+-ion-doped upconversion nanoprobes: relaxivity mechanism probing and sensitivity optimization. Adv Funct Mater 23(3):298–307. doi:10.1002/adfm.201201469
12. Xiao Q, Bu W, Ren Q, Zhang S, Xing H, Chen F, Li M, Zheng X, Hua Y, Zhou L, Peng W, Qu H, Wang Z, Zhao K, Shi J (2012) Radiopaque fluorescence-transparent TaOx decorated upconversion nanophosphors for in vivo CT/MR/UCL trimodal imaging. Biomaterials 33(30):7530–7539. doi:10.1016/j.biomaterials.2012.06.028
13. Xing H, Bu W, Ren Q, Zheng X, Li M, Zhang S, Qu H, Wang Z, Hua Y, Zhao K, Zhou L, Peng W, Shi J (2012) A NaYbF4: Tm^{3+} nanoprobe for CT and NIR-to-NIR fluorescent bimodal imaging. Biomaterials 33(21):5384–5393. doi:10.1016/j.biomaterials.2012.04.002
14. Sun Y (2013) Upconversion nanophosphors Naluf4:Yb, Tm for lymphatic imaging in vivo by real-time upconversion luminescence imaging under ambient light and high-resolution x-ray CT. Theranostics 3(5):346–353. doi:10.7150/thno.5137
15. Xing H, Zheng X, Ren Q, Bu W, Ge W, Xiao Q, Zhang S, Wei C, Qu H, Wang Z, Hua Y, Zhou L, Peng W, Zhao K, Shi J (2013) Computed tomography imaging-guided radiotherapy by targeting upconversion nanocubes with significant imaging and radiosensitization enhancements. Sci Rep:3:1751. doi:10.1038/srep01751
16. Sun Y, Yu M, Liang S, Zhang Y, Li C, Mou T, Yang W, Zhang X, Li B, Huang C, Li F (2011) Fluorine-18 labeled rare-earth nanoparticles for positron emission tomography (PET) imaging of sentinel lymph node. Biomaterials 32(11):2999–3007. doi:10.1016/j.biomaterials.2011.01.011
17. Liu Q, Sun Y, Li C, Zhou J, Li C, Yang T, Zhang X, Yi T, Wu D, Li F (2011) ^{18}F-labeled magnetic-upconversion nanophosphors via rare-earth cation-assisted ligand assembly. ACS Nano 5(4):3146–3157
18. Sun Y, Zhu X, Peng J, Li F (2013) Core-shell lanthanide upconversion nanophosphors as four-modal probes for tumor angiogenesis imaging. ACS Nano 7(12):11290–11300
19. Yang Y, Sun Y, Cao T, Peng J, Liu Y, Wu Y, Feng W, Zhang Y, Li F (2013) Hydrothermal synthesis of NaLuF4:153Sm, Yb, Tm nanoparticles and their application in dual-modality upconversion luminescence and SPECT bioimaging. Biomaterials 34(3):774–783. doi:10.1016/j.biomaterials.2012.10.022
20. Wang C, Cheng L, Liu Z (2011) Drug delivery with upconversion nanoparticles for multifunctional targeted cancer cell imaging and therapy. Biomaterials 32(4):1110–1120. doi:10.1016/j.biomaterials.2010.09.069
21. Hou Z, Li C, Ma PA, Cheng Z, Li X, Zhang X, Dai Y, Yang D, Lian H, Lin J (2012) Up-conversion luminescent and porous NaYF4:Yb3+, Er3+@SiO2 nanocomposite fibers for anti-cancer drug delivery and cell imaging. Adv Funct Mater 22(13):2713–2722. doi:10.1002/adfm.201200082
22. Yunlu Dai, Ping'an Ma, Ziyong Cheng, Xiaojiao Kang, Xiao Zhang, Zhiyao Hou, Chunxia Li, Dongmei Yang, Xuefeng Zhai, Lin J (2012) Up-conversion cell imaging and pH induced

thermally controlled drug release from NaYF4:Yb3+/Er3+@Hydrogel core/shell hybrid microspheres. ACS Nano 6(4):3327–3338
23. Xiao Q, Ji Y, Xiao Z, Zhang Y, Lin H, Wang Q (2013) Novel multifunctional NaYF4:Er3+, Yb3+/PEGDA hybrid microspheres: NIR-light-activated photopolymerization and drug delivery. Chem Commun 49(15):1527. doi:10.1039/c2cc37620b
24. Ungun B, Prud'homme RK, Budijono SJ, Shan J, Lim SF, Yiguang J, Austin R (2009) Nanofabricated upconversion nanoparticles for photodynamic therapy. Opt Express 17(1):80–86
25. Qian HS, Guo HC, Ho PC-L, Mahendran R, Zhang Y (2009) Mesoporous-silica-coated up-conversion fluorescent nanoparticles for photodynamic therapy. Small 5(20):2285–2290. doi:10.1002/smll.200900692
26. Wang C, Tao H, Cheng L, Liu Z (2011) Near-infrared light induced in vivo photodynamic therapy of cancer based on upconversion nanoparticles. Biomaterials 32:6145–6154. doi:10.1016/j.biomaterials.2011.05.007
27. Shan J, Budijono SJ, Hu G, Yao N, Kang Y, Ju Y, Prud'homme RK (2011) Pegylated composite nanoparticles containing upconverting phosphors and meso-tetraphenyl porphine (TPP) for photodynamic therapy. Adv Funct Mater 21(13):2488–2495. doi:10.1002/adfm.201002516
28. Liu X, Zheng M, Kong X, Zhang Y, Zeng Q, Sun Z, Buma WJ, Zhang H (2013) Separately doped upconversion-C60 nanoplatform for NIR imaging-guided photodynamic therapy of cancer cells. Chem Commun 49(31):3224. doi:10.1039/c3cc41013g
29. Zhang T, Ge J, Hu Y, Yin Y (2007) A general approach for transferring hydrophobic nanocrystals into water. Nano Lett 7(10):3203–3207
30. Boyer J-C, Manseau M-P, Murray JI, van Veggel FCJM (2010) Surface modification of upconverting NaYF4Nanoparticles with PEG–phosphate ligands for NIR (800 nm) biolabeling within the biological window. Langmuir 26(2):1157–1164. doi:10.1021/la902260j
31. Johnson NJJ, Sangeetha NM, Boyer J-C, van Veggel FCJM (2010) Facile ligand-exchange with polyvinylpyrrolidone and subsequent silica coating of hydrophobic upconverting β-NaYF4:Yb3+/Er3+ nanoparticles. Nanoscale 2(5):771. doi:10.1039/b9nr00379g
32. Chen Z, Chen H, Hu H, Yu M, Li F, Zhang Q, Zhou Z, Yi T, Huang C (2008) Versatile synthesis strategy for carboxylic acid-functionalized upconverting nanophosphors as biological labels. J Am Chem Soc 130:3023–3029
33. Yang D, Dai Y, Ma P, Kang X, Shang M, Cheng Z, Li C, Lin J (2012) Synthesis of Li1–xNaxYF4:Yb3+/Ln3+ ($0 \leq x \leq 0.3$, Ln = Er, Tm, Ho) nanocrystals with multicolor upconversion luminescence properties for in vitro cell imaging. J Mater Chem 22(38):20618. doi:10.1039/c2jm33910b
34. Wang L, Yan R, Huo Z, Wang L, Zeng J, Bao J, Wang X, Peng Q, Li Y (2005) Fluorescence resonant energy transfer biosensor based on upconversion-luminescent nanoparticles. Angew Chem Int Ed 44(37):6054–6057. doi:10.1002/anie.200501907
35. Yi G, Peng Y, Gao Z (2011) Strong red-emitting near-infrared-to-visible upconversion fluorescent nanoparticles. Chem Mater 23(11):2729–2734. doi:10.1021/cm103175s
36. Zhang Q, Song K, Zhao J, Kong X, Sun Y, Liu X, Zhang Y, Zeng Q, Zhang H (2009) Hexanedioic acid mediated surface–ligand-exchange process for transferring NaYF4:Yb/Er (or Yb/Tm) up-converting nanoparticles from hydrophobic to hydrophilic. J Colloid Interface Sci 336(1):171–175. doi:10.1016/j.jcis.2009.04.024
37. Kumar R, Nyk M, Ohulchanskyy TY, Flask CA, Prasad PN (2009) Combined optical and MR bioimaging using rare earth ion doped NaYF4Nanocrystals. Adv Funct Mater 19(6):853–859. doi:10.1002/adfm.200800765
38. Zhan Q, Qian J, Liang H, Somesfalean G, Wang D, He S, Zhang Z, Andersson-Engels S (2011) Using 915 nm laser excited $Tm^{3+}/Er^{3+}/Ho^{3+}$-Doped $NaYbF_4$ upconversion nanoparticles for in vitro and deeper in vivo bioimaging without overheating irradiation. ACS Nano 5(5):3744–3757
39. Bogdan N, Vetrone F, Roy R, Capobianco JA (2010) Carbohydrate-coated lanthanide-doped upconverting nanoparticles for lectin recognition. J Mater Chem 20(35):7543. doi:10.1039/c0jm01617a

40. Wang M, Liu J-L, Zhang Y-X, Hou W, Wu X-L, Xu S-K (2009) Two-phase solvothermal synthesis of rare-earth doped NaYF4 upconversion fluorescent nanocrystals. Mater Lett 63(2):325–327. doi:10.1016/j.matlet.2008.10.028
41. Bogdan N, Vetrone F, Ozin GA, Capobianco JA (2011) Synthesis of ligand-free colloidally stable water dispersible brightly luminescent lanthanide-doped upconverting nanoparticles. Nano Lett 11(2):835–840. doi:10.1021/nl1041929
42. Bogdan N, Rodríguez EM, Sanz-Rodríguez F, Iglesias de la Cruz MC, Juarranz Á, Jaque D, Solé JG, Capobianco JA (2012) Bio-functionalization of ligand-free upconverting lanthanide doped nanoparticles for bio-imaging and cell targeting. Nanoscale 4(12):3647. doi:10.1039/c2nr30982c
43. Liu J-n, Bu W, Pan L-m, Zhang S, Chen F, Zhou L, Zhao K-L, Peng W, Shi J (2012) Simultaneous nuclear imaging and intranuclear drug delivery by nuclear-targeted multifunctional upconversion nanoprobes. Biomaterials 33(29):7282–7290. doi:10.1016/j.biomaterials.2012.06.035
44. Sivakumar S, Diamente PR, van Veggel FCJM (2006) Silica-coated Ln3+-doped LaF3 nanoparticles as robust down- and upconverting biolabels. Chem Eur J 12(22):5878–5884. doi:10.1002/chem.200600224
45. Das GK, Heng BC, Ng S-C, White T, Loo JSC, D'Silva L, Padmanabhan P, Bhakoo KK, Selvan ST, Tan TTY (2010) Gadolinium oxide ultranarrow nanorods as multimodal contrast agents for optical and magnetic resonance imaging. Langmuir 26(11):8959–8965. doi:10.1021/la903512m, 10.1021/la904751q, 10.1021/la902260j, 10.1002/jbm.a.32533
46. Hu H, Xiong L, Zhou J, Li F, Cao T, Huang C (2009) Multimodal-luminescence core-shell nanocomposites for targeted imaging of tumor cells. Chem Eur J 15(14):3577–3584. doi:10.1002/chem.200802261
47. Abdul Jalil R, Zhang Y (2008) Biocompatibility of silica coated NaYF4 upconversion fluorescent nanocrystals. Biomaterials 29(30):4122–4128. doi:10.1016/j.biomaterials.2008.07.012
48. Li Z, Wang L, Wang Z, Liu X, Xiong Y (2011) Modification of NaYF4:Yb, Er@SiO2Nanoparticles with gold nanocrystals for tunable green-to-red upconversion emissions. J Phys Chem C 115(8):3291–3296. doi:10.1021/jp110603r
49. Liu Z, Yi G, Zhang H, Ding J, Zhang Y, Xue J (2008) Monodisperse silica nanoparticles encapsulating upconversion fluorescent and superparamagnetic nanocrystals. Chem Commun 6:694. doi:10.1039/b715402j
50. Li Z, Zhang Y, Jiang S (2008) Multicolor core/shell-structured upconversion fluorescent nanoparticles. Adv Mater 20(24):4765–4769. doi:10.1002/adma.200801056
51. Xing H, Bu W, Zhang S, Zheng X, Li M, Chen F, He Q, Zhou L, Peng W, Hua Y, Shi J (2012) Multifunctional nanoprobes for upconversion fluorescence, MR and CT trimodal imaging. Biomaterials 33(4):1079–1089. doi:10.1016/j.biomaterials.2011.10.039
52. Liu J, Bu W, Zhang S, Chen F, Xing H, Pan L, Zhou L, Peng W, Shi J (2012) Controlled synthesis of uniform and monodisperse upconversion core/mesoporous silica shell nanocomposites for bimodal imaging. Chem Eur J 18(8):2335–2341. doi:10.1002/chem.201102599
53. Li C, Hou Z, Dai Y, Yang D, Cheng Z, Ma P, Lin J (2013) A facile fabrication of upconversion luminescent and mesoporous core–shell structured β-NaYF4:Yb3+, Er3+@mSiO2 nanocomposite spheres for anti-cancer drug delivery and cell imaging. Biomater Sci 1:213–223. doi:10.1039/c2bm00087c
54. Wang F, Liu X (2009) Recent advances in the chemistry of lanthanide-doped upconversion nanocrystals. Chem Soc Rev 38(4):976. doi:10.1039/b809132n
55. Yu X, Li M, Xie M, Chen L, Li Y, Wang Q (2010) Dopant-controlled synthesis of water-soluble hexagonal NaYF4 nanorods with efficient upconversion fluorescence for multicolor bioimaging. Nano Res 3(1):51–60. doi:10.1007/s12274-010-1008-2
56. Cheng L, Yang K, Zhang S, Shao M, Lee S, Liu Z (2010) Highly-sensitive multiplexed in vivo imaging using pegylated upconversion nanoparticles. Nano Res 3(10):722–732. doi:10.1007/s12274-010-0036-2

57. Ren G, Zeng S, Hao J (2011) Tunable multicolor upconversion emissions and paramagnetic property of monodispersed bifunctional lanthanide-doped NaGdF4Nanorods. J Phys Chem C 115(41):20141–20147. doi:10.1021/jp2064529
58. Jeong S, Won N, Lee J, Bang J, Yoo J, Kim SG, Chang JA, Kim J, Kim S (2011) Multiplexed near-infrared in vivo imaging complementarily using quantum dots and upconverting NaYF4:Yb3+, Tm3+ nanoparticles. Chem Commun 47(28):8022. doi:10.1039/c1cc12746b
59. Idris NM, Li Z, Ye L, Wei Sim EK, Mahendran R, Ho PC-L, Zhang Y (2009) Tracking transplanted cells in live animal using upconversion fluorescent nanoparticles. Biomaterials 30(28):5104–5113. doi:10.1016/j.biomaterials.2009.05.062
60. Liu Q, Sun Y, Yang T, Feng W, Li C, Li F (2011) Sub-10 nm hexagonal lanthanide-doped NaLuF4 Upconversion nanocrystals for sensitive bioimaging in vivo. J Am Chem Soc 133(43):17122–17125. doi:10.1021/ja207078s
61. Wang C, Cheng L, Xu H, Liu Z (2012) Towards whole-body imaging at the single cell level using ultra-sensitive stem cell labeling with oligo-arginine modified upconversion nanoparticles. Biomaterials 33(19):4872–4881. doi:10.1016/j.biomaterials.2012.03.047
62. Cheng L, Wang C, Ma X, Wang Q, Cheng Y, Wang H, Li Y, Liu Z (2013) Multifunctional upconversion nanoparticles for dual-modal imaging-guided stem cell therapy under remote magnetic control. Adv Funct Mater 23(3):272–280. doi:10.1002/adfm.201201733
63. Xiong L-Q, Chen Z-G, Yu M-X, Li F-Y, Liu C, Huang C-H (2009) Synthesis, characterization, and in vivo targeted imaging of amine-functionalized rare-earth up-converting nanophosphors. Biomaterials 30(29):5592–5600. doi:10.1016/j.biomaterials.2009.06.015
64. Xiong L, Chen Z, Tian Q, Cao T, Xu C, Li F (2009) High contrast upconversion luminescence targeted imaging in vivo using peptide-labeled nanophosphors. Anal Chem 81(21):8687–8694. doi:10.1021/ac901960d
65. Ni D, Zhang J, Bu W, Xing H, Han F, Xiao Q, Yao Z, Chen F, He Q, Liu J, Zhang S, Fan W, Zhou L, Peng W, Shi J (2014) Dual-targeting upconversion nanoprobes across the blood-brain barrier for magnetic resonance/fluorescence imaging of intracranial glioblastoma. ACS Nano 8(2):1231–1242
66. Hilderbrand SA, Shao F, Salthouse C, Mahmood U, Weissleder R (2009) Upconverting luminescent nanomaterials: application to in vivo bioimaging. Chem Commun 28:4188. doi:10.1039/b905927j
67. Xing H, Zhang S, Bu W, Zheng X, Wang L, Xiao Q, Ni D, Zhang J, Zhou L, Peng W, Zhao K, Hua Y, Shi J (2014) Ultrasmall NaGdF4Nanodots for efficient MR angiography and atherosclerotic plaque imaging. Adv Mater 26(23):3867–3872. doi:10.1002/adma.201305222
68. Kobayashi H, Kosaka N, Ogawa M, Morgan NY, Smith PD, Murray CB, Ye X, Collins J, Kumar GA, Bell H, Choyke PL (2009) In vivo multiple color lymphatic imaging using upconverting nanocrystals. J Mater Chem 19(36):6481. doi:10.1039/b910512c
69. Cao T, Yang Y, Gao Y, Zhou J, Li Z, Li F (2011) High-quality water-soluble and surface-functionalized upconversion nanocrystals as luminescent probes for bioimaging. Biomaterials 32(11):2959–2968
70. Moulder JE, Rockwell S (1987) Tumor hypoxia: its impact on cancer therapy. Cancer Metastasis Rev 5(4):313–341
71. Liu J, Liu Y, Bu W, Bu J, Sun Y, Du J, Shi J (2014) Ultrasensitive nanosensors based on upconversion nanoparticles for selective hypoxia imaging in vivo upon near-infrared excitation. J Am Chem Soc 136(27):9701–9709. doi:10.1021/ja5042989
72. Zhou J, Sun Y, Du X, Xiong L, Hu H, Li F (2010) Dual-modality in vivo imaging using rare-earth nanocrystals with near-infrared to near-infrared (NIR-to-NIR) upconversion luminescence and magnetic resonance properties. Biomaterials 31(12):3287–3295. doi:10.1016/j.biomaterials.2010.01.040
73. Zhou L, Gu Z, Liu X, Yin W, Tian G, Yan L, Jin S, Ren W, Xing G, Li W, Chang X, Hu Z, Zhao Y (2012) Size-tunable synthesis of lanthanide-doped Gd2O3 nanoparticles and their applications for optical and magnetic resonance imaging. J Mater Chem 22(3):966. doi:10.1039/c1jm13758a

74. Tian G, Gu Z, Zhou L, Yin W, Liu X, Yan L, Jin S, Ren W, Xing G, Li S, Zhao Y (2012) Mn2+ dopant-controlled synthesis of NaYF4:Yb/Er upconversion nanoparticles for in vivo imaging and drug delivery. Adv Mater 24(9):1226–1231. doi:10.1002/adma.201104741
75. Chen F, Bu W, Zhang S, Liu X, Liu J, Xing H, Xiao Q, Zhou L, Peng W, Wang L, Shi J (2011) Positive and negative lattice shielding effects co-existing in Gd (III) ion doped bifunctional upconversion nanoprobes. Adv Funct Mater 21(22):4285–4294. doi:10.1002/adfm.201101663
76. Wang F, Wang J, Liu X (2010) Direct evidence of a surface quenching effect on size-dependent luminescence of upconversion nanoparticles. Angew Chem Int Ed 49(41):7456–7460. doi:10.1002/anie.201003959
77. Zhang F, Che R, Li X, Yao C, Yang J, Shen D, Hu P, Li W, Zhao D (2012) Direct imaging the upconversion nanocrystal core/shell structure at the subnanometer level: shell thickness dependence in upconverting optical properties. Nano Lett 12(6):2852–2858. doi:10.1021/nl300421n
78. Chen F, Zhang S, Bu W, Liu X, Chen Y, He Q, Zhu M, Zhang L, Zhou L, Peng W, Shi J (2010) A "neck-formation" strategy for an antiquenching magnetic/upconversion fluorescent bimodal cancer probe. Chem Eur J 16(37):11254–11260. doi:10.1002/chem.201000525
79. Xia A, Gao Y, Zhou J, Li C, Yang T, Wu D, Wu L, Li F (2011) Core–shell NaYF4:Yb3+, Tm3+@FexOy nanocrystals for dual-modality T2-enhanced magnetic resonance and NIR-to-NIR upconversion luminescent imaging of small-animal lymphatic node. Biomaterials 32(29):7200–7208. doi:10.1016/j.biomaterials.2011.05.094
80. Cheng L, Yang K, Li Y, Zeng X, Shao M, Lee S-T, Liu Z (2012) Multifunctional nanoparticles for upconversion luminescence/MR multimodal imaging and magnetically targeted photothermal therapy. Biomaterials 33(7):2215–2222. doi:10.1016/j.biomaterials.2011.11.069
81. Zhang F, Braun GB, Pallaoro A, Zhang Y, Shi Y, Cui D, Moskovits M, Zhao D, Stucky GD (2012) Mesoporous multifunctional upconversion luminescent and magnetic "Nanorattle" materials for targeted chemotherapy. Nano Lett 12(1):61–67. doi:10.1021/nl202949y
82. Das GK, Johnson NJJ, Cramen J, Blasiak B, Latta P, Tomanek B, van Veggel FCJM (2012) NaDyF4Nanoparticles as T2Contrast agents for ultrahigh field magnetic resonance imaging. J Phys Chem Lett 3(4):524–529. doi:10.1021/jz201664h
83. Lee N, Choi SH, Hyeon T (2013) Nano-sized CT contrast agents. Adv Mater. doi:10.1002/adma.201300081
84. Liu Z, Pu F, Huang S, Yuan Q, Ren J, Qu X (2013) Long-circulating Gd2O3:Yb3+, Er3+ upconversion nanoprobes as high-performance contrast agents for multi-modality imaging. Biomaterials 34(6):1712–1721. doi:10.1016/j.biomaterials.2012.11.009
85. Xia A, Chen M, Gao Y, Wu D, Feng W, Li F (2012) Gd3+ complex-modified NaLuF4-based upconversion nanophosphors for trimodality imaging of NIR-to-NIR upconversion luminescence, X-Ray computed tomography and magnetic resonance. Biomaterials 33(21):5394–5405. doi:10.1016/j.biomaterials.2012.04.025
86. Zhu X, Zhou J, Chen M, Shi M, Feng W, Li F (2012) Core–shell Fe3O4@NaLuF4:Yb, Er/Tm nanostructure for MRI, CT and upconversion luminescence tri-modality imaging. Biomaterials 33(18):4618–4627. doi:10.1016/j.biomaterials.2012.03.007
87. Ni D, Bu W, Zhang S, Zheng X, Li M, Xing H, Xiao Q, Liu Y, Hua Y, Zhou L, Peng W, Zhao K, Shi J (2014) Single Ho3+-doped upconversion nanoparticles for high-performanceT2-weighted brain tumor diagnosis and MR/UCL/CT multimodal imaging. Adv Funct Mater 24(42):6613–6620. doi:10.1002/adfm.201401609
88. Zhou J, Yu M, Sun Y, Zhang X, Zhu X, Wu Z, Wu D, Li F (2011) Fluorine-18-labeled Gd3+/Yb3+/Er3+ co-doped NaYF4 nanophosphors for multimodality PET/MR/UCL imaging. Biomaterials 32(4):1148–1156. doi:10.1016/j.biomaterials.2010.09.071
89. Zhang P, Steelant W, Kumar M, Scholfield M (2007) Versatile photosensitizers for photodynamic therapy at infrared excitation. J Am Chem Soc 129:4526–4527
90. Zhao Z, Han Y, Lin C, Hu D, Wang F, Chen X, Chen Z, Zheng N (2012) Multifunctional core-shell upconverting nanoparticles for imaging and photodynamic therapy of liver cancer cells. Chem Asian J 7(4):830–837. doi:10.1002/asia.201100879

91. Chen F, Zhang S, Bu W, Chen Y, Xiao Q, Liu J, Xing H, Zhou L, Peng W, Shi J (2012) A uniform sub-50 nm-sized magnetic/upconversion fluorescent bimodal imaging agent capable of generating singlet oxygen by using a 980 nm laser. Chem Eur J 18:7082–7090. doi:10.1002/chem.201103611
92. Qiao X-F, Zhou J-C, Xiao J-W, Wang Y-F, Sun L-D, Yan C-H (2012) Triple-functional core–shell structured upconversion luminescent nanoparticles covalently grafted with photosensitizer for luminescent, magnetic resonance imaging and photodynamic therapy in vitro. Nanoscale 4(15):4611–4623. doi:10.1039/c2nr30938f
93. Liu K, Liu X, Zeng Q, Zhang Y, Tu L, Liu T, Kong X, Wang Y, Cao F, Lambrechts SAG, Aalders MCG, Zhang H (2012) Covalently assembled NIR nanoplatform for simultaneous fluorescence imaging and photodynamic therapy of cancer cells. ACS Nano 6(5):4054–4062
94. Park YI, Kim HM, Kim JH, Moon KC, Yoo B, Lee KT, Lee N, Choi Y, Park W, Ling D, Na K, Moon WK, Choi SH, Park HS, Yoon S-Y, Suh YD, Lee SH, Hyeon T (2012) Theranostic probe based on lanthanide-doped nanoparticles for simultaneous in vivo dual-modal imaging and photodynamic therapy. Adv Mater 24(42):5755–5761. doi:10.1002/adma.201202433
95. Idris NM, Gnanasammandhan MK, Zhang J, Ho PC, Mahendran R, Zhang Y (2012) In vivo photodynamic therapy using upconversion nanoparticles as remote-controlled nanotransducers. Nat Med 18(10):1580–1585. doi:10.1038/nm.2933
96. Juzenas P, Chen W, Sun Y-P, Coelho MAN, Generalov R, Generalova N, Christensen IL (2008) Quantum dots and nanoparticles for photodynamic and radiation therapies of cancer. Adv Drug Deliv Rev 60(15):1600–1614. doi:10.1016/j.addr.2008.08.004
97. Ridder MD, Esch GV, Engels B, Verovskl V, Storme G (2008) Hypoxic tumor cell radiosensitization: role of the iNOS/NO pathway. Bull Cancer 95(3):282–291. doi:10.1684/bdc.2008.0592
98. Hainfeld JF, Dilmanian FA, Slatkin DN, Smilowitz HM (2008) Radiotherapy enhancement with gold nanoparticles. J Pharm Pharmacol 60(8):977–985. doi:10.1211/jpp.60.8.0005
99. Tian G, Ren W, Yan L, Jian S, Gu Z, Zhou L, Jin S, Yin W, Li S, Zhao Y (2013) Red-emitting upconverting nanoparticles for photodynamic therapy in cancer cells under near-infrared excitation. Small 9(11):1929–1938. doi:10.1002/smll.201201437
100. Fan W, Shen B, Bu W, Chen F, Zhao K, Zhang S, Zhou L, Peng W, Xiao Q, Xing H, Liu J, Ni D, He Q, Shi J (2013) Rattle-structured multifunctional nanotheranostics for synergetic chemo-/radiotherapy and simultaneous magnetic/luminescent dual-mode imaging. J Am Chem Soc 135(17):6494–6503. doi:10.1021/ja312225b
101. Fan W, Shen B, Bu W, Chen F, He Q, Zhao K, Zhang S, Zhou L, Peng W, Xiao Q, Ni D, Liu J, Shi J (2014) A smart upconversion-based mesoporous silica nanotheranostic system for synergetic chemo-/radio-/photodynamic therapy and simultaneous MR/UCL imaging. Biomaterials 35(32):8992–9002. doi:10.1016/j.biomaterials.2014.07.024